Mississippi State University

Scholars Junction

8-7-2020

Investigating the presence of stellar companions around hot Jupiter host stars using MagAO.

Farzaneh Zohrabi

Follow this and additional works at: https://scholarsjunction.msstate.edu/td

Investigating the presence of stellar companions around hot Jupiter host stars using MagAO

By

Farzaneh Zohrabi

Approved by:

Angelle Tanner (Major Professor)
Donna M. Pierce
Jeff Winger
Henk F. Arnoldus (Graduate Coordinator)
Rick Travis (Dean, College of Arts & Sciences)

A Thesis
Submitted to the Faculty of
Mississippi State University
in Partial Fulfillment of the Requirements
for the Degree of Master of Science
in Physics
in the Department of Physics and Astronomy

Mississippi State, Mississippi
August 2020

Name: Farzaneh Zohrabi

Date of Degree: August 7, 2020

Institution: Mississippi State University

Major Field: Physics

Major Professor: Angelle M. Tanner

Title of Study: Investigating the presence of stellar companions around hot Jupiter host stars using MagAO.

Pages in Study: 53

Candidate for Degree of Master of Science

In this work, we investigate the presence of stellar companions around hot Jupiter system using data sets from the Clio and VISAO instruments on Magellan Telescope. We observed eighteen targets of which eleven have known spin-orbit obliquity measurements. We detected eleven candidate companions of which five are new discoveries, five involved the validation and confirmation of previous studies, and one candidate proved to be a background star not bound to the transiting planet system. Out of eleven systems with known spin-orbit obliquity seven systems have candidate companions. Due to size of the sample we could not find any correlation between the spin-orbit obliquity and the presence of a stellar companion. As future work, we will do follow up observations on the targets with candidate companions. We will increase our sample to one hundred systems to investigate if there is correlation between spin-orbit obliquity and presence of a distant stellar companion.

DEDICATION

To my supportive beloved sisters, parents, and partner who without them I couldn't follow my

dreams.

ACKNOWLEDGEMENTS

TABLE OF CONTENTS

LIST OF TABLES

LIST OF FIGURES

CHAPTER I

INTRODUCTION

1.1 Exoplanetary Science

An exoplanet, or an extra-solar planet, is the term that scientists use for planets outside the Solar System. Before discovering the first exoplanet, for hundreds of years, people wondered if the planets in our solar system are the only planets in the universe or there are planets around other stars too. Finding and characterizing extra-solar planets is now a hot topic in astronomy since this is our only path for searching for life outside our planet Earth.

The Solar System has been our only well studied observational sample for a very long time before the discovery of the first extra-solar planets. Exploring the Solar System led us to the planet formation theories, which proposed that planets form from a gas and dust cloud which collapses into a disk. In this inhomogeneous protoplanetary disk, different materials have different temperatures, which leads to having different planets in the system. The order of the planets in a Solar System is related to its formation process. All the rocky cores (proto-planets) beyond the snow/frost line (the snow/frost line is the minimum radius from the main star in the system that water, methane, carbon dioxide, etc. could condense into solid ice grains (Podolak & Zucker, 2004)) grew quickly and accumulated massive gaseous atmospheres before the gas disk dissipated. In the inner disk (inner to the snow line), the planet formation was slower, and the rocky cores were not big enough to accrete their gaseous atmosphere before the dissipation of the gas disk. Planets usually stay in their original orbit in which they formed. Typically, the rocky and coplanar

planets are inside the frost line, and the gas giants form beyond the frost line (Mordasini et al., 2015).

51 Pegasus B, was the first extra-solar planet discovered in 1995, that orbits around a main-sequence star. (Mayor & Queloz, 1995). This discovery challenged our planet formation theories that we had based on our Solar System. It is a close-in orbit gas giant, which orbits its star ten times closer than Mercury's orbits the Sun (instead of being several AU away from its host star). Based on solar system planets formation studies, the gas giant planets belong to beyond the snow line.

51 Peg B belongs to a type of planet known as hot Jupiters. Discovery of 51 Peg B and other hot Jupiters showed us that planet formation theories needed revolutionary changes. Hot Jupiters are the one exoplanet type that questioned our understanding of the formation and evolution of planetary systems with their properties.

1.2   Hot Jupiters

Hot Jupiters are gas giant planets with astonishing close-in orbits (periods of 3 to 10 days). They are the easiest exoplanets to be detected by the radial velocity method because of their large mass and short period. At least 10%-15% of Sun-like stars host a Jovian-mass planet; however, hot Jupiters with a semi-major axis of less than 0.1 AU have been detected around ~ 1% of solar-type stars (Wu et al., 2007). Astronomers believe that hot Jupiters form several AU away from their host stars, and they migrate into their close-in orbit. Still, the reason for such migration needs to be supported by a strong theory that could explain all hot Jupiter's properties. At the time of this writing, about 20 years after the discovery of the first hot Jupiters, no theory has been proved to

be an explanation for all properties, origin, and formation of hot Jupiters. That's why there are some different formation theories for the origin of hot Jupiters.

Through observation and measurements of high stellar obliquities of transiting hot Jupiters in the last few years, many exoplanets are proven to have planetary orbit misalignment with respect to the spin axis of their host stars (Winn & Fabrycky, 2015). Three main theories tried to explain the mysterious origin story of hot Jupiters, including; in situ formation(Dawson & Johnson, 2018), gas disk migration(Dawson & Johnson, 2018), and high-eccentricity tidal migration (Dong et al., 2013; Mustill et al., 2015; Carrera et al., 2019).

1.2.1   Hot Jupiter properties

Hot Jupiters are mostly known for their large mass and short orbital periods. The hot Jupiters mass can be in a range of 0.36 to 11.8 M_{Jup}. The mass limit for exoplanets is 13.6 M_{Jup} since this is the boundary before the planet turns into a brown dwarf (Chauvin et al., 2005). The period of hot Jupiters is usually in a range of 1.6 to 111 Earth days. (Winn et al., 2010).

The orbit of hot Jupiters with a period of about three or fewer days is usually low eccentric and nearly circular. They typically keep one side toward the host star, being tidally locked. Also, hot Jupiters are not found to have low-mass and close-in planetary companions.

The first few years from the hot Jupiters discovery, astronomers believed these gas giants have well-aligned orbits around their host stars. Still, after measuring the sky-projected obliquity of hot Jupiters, they noticed many have spin-orbit misalignments (Figure 1.1) (Chauvin et al., 2005). Spin-orbit obliquity (λ) is the angle between the host star's spin axis and the planet's angular momentum vector (see Figure 1.1). The sky projected obliquity (λ) is the projected angle between the axis of sky rotation and the planetary orbit.

Sky-projected obliquity (λ) is measured spectroscopically using the Rossiter–McLaughlin effect. Rossiter–McLaughlin effect measures the distortion in the radial velocity stellar spectra caused by a transiting exoplanet (Queloz et al., 2000). However, there are many ways to measure the obliquity such as the gravity-darkening method (Barnes, 2009), the asteroseismic method (Chaplin et al., 2013; Stello et al., 2013; Van Eylen et al., 2014), the photometric variability method (Mazeh, Perets, et al., 2015), and the spot-crossing anomalies method (Désert et al., 2011; Mazeh, Holczer, et al., 2015; Sanchis-Ojeda & Winn, 2011).
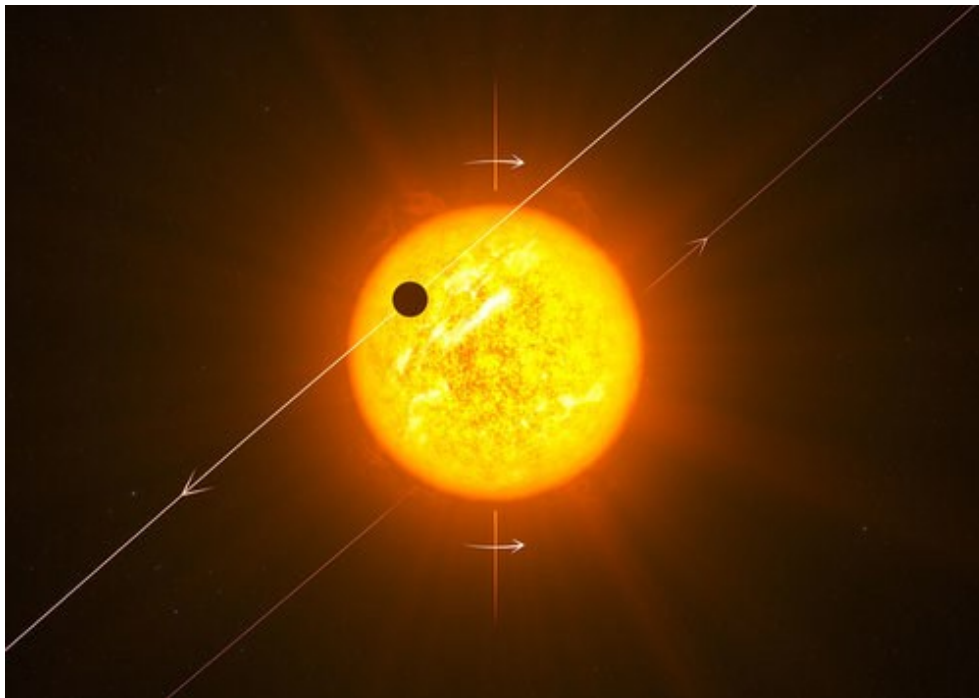
Figure 1.1   Spin-orbit misalignment in which the orbit of the planet is not aligned with the spin axis of the star (Image Credit: ESO/L. Calcada)

1.2.2   Hot Jupiters origin and formation theories

Three primary theories partially explain the hot Jupiters properties. Unfortunately, these theories are not able to explain the origin of hot Jupiters thoroughly including the observed prevalence of spin-orbit misalignments.

1.2.2.1   In situ formation

In this theory the hot Jupiters are hypothesized to have been formed in the orbit in which they are currently observed instead of migrating from another orbit. (Dawson & Johnson, 2018)

1.2.2.2   Gas disk migration

In this theory, the hot Jupiters are forming beyond the snow line in a wide orbit around the host star. The theory states that the hot Jupiters migrate inward to a short period orbit because of torques from the gaseous proto-planetary disk and the interactions between the planet and this disk. (Dawson & Johnson, 2018)

1.2.2.3   High-eccentricity tidal migration

This theory states that hot Jupiters form in wide orbits with semi-major axis of several to hundreds of AU from their host star and then migrate inward well after they formed. Planets need to go through two steps to turn from a cold Jupiter in an outer orbit to a hot Jupiter with close-in orbit. First, the exoplanet needs to reduce its orbital angular momentum and then reduce its orbital energy. As Figure 1.2 shows, high-eccentricity tidal migration proposes a third body (a planet or a distant stellar companion) perturbs the hot Jupiter's orbit while extracting the orbital angular momentum and forcing it to a highly elliptical orbit and this is followed by tidal dissipation of the exoplanet's energy which circularizes the orbit. High-eccentricity migration may provide a better

explanation for the hot Jupiter's spin-orbit misalignments (Désert et al., 2011; Mazeh, Holczer, et al., 2015; Sanchis-Ojeda & Winn, 2011). This theory requires that hot Jupiters have (or had in the past) planetary or stellar companions in wide orbits, and indeed recent studies estimate that around 70% of hot Jupiters have giant planets or stars as a companion in wide orbits (Knutson et al., 2014; Ngo et al., 2015). There are several mechanisms which propose an explanation for planetary migration and spin-orbit misalignments such as planet-planet scattering (Chatterjee et al., 2008), secular chaos (Naoz et al., 2011; Wu & Lithwick, 2011), and Kozai mechanism (Naoz et al., 2012; Wu et al., 2007).

A study in 2015 showed that high-eccentricity migration of a gas giant planet would remove any pre-existing planets in orbits of a few tenths of an AU in the system, therefore usually, there is no evidence for a close-in companion for hot Jupiters. This fact also supports the high-eccentricity theory as migration through a protoplanetary gas disk usually does not suppress planet formation.(Fogg & Nelson, 2007; Ketchum et al., 2011; Ogihara et al., 2014). However, it is unknown which mechanism(s) of high-eccentricity (planet-planet scattering, the Kozai effect, or low-inclination secular interactions) is responsible for this pre-existing planet destruction (Mustill et al., 2015).
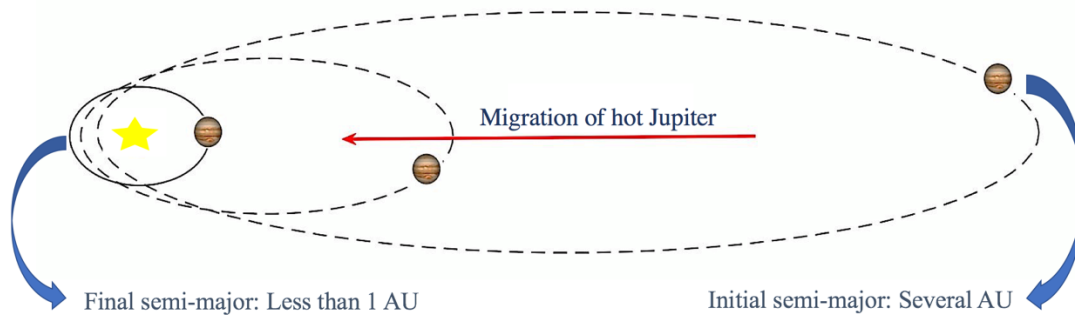
Figure 1.2   High-eccentricity tidal migration in which the hot Jupiter migrates from its original wide orbit to a close-in orbit due to gravitational interactions between the planet and a distant companion. (Image Credit: Farzaneh Zohrabi)

1.2.2.3.1   Planet-planet scattering

Planet– planet scattering is a primary dynamical mechanism able to alter significantly the structure of a planetary system. Gravitational interactions between planets in a planetary system lead to an evolution in orbital properties, which can cause planet orbits to cross. In the planetary systems with gas giants, they typically gravitationally scatter instead of colliding.

Recently a study by Daniel Carrera et al. modeled in 2019 the dynamical evolution of unstable planetary systems with three Jupiter-mass exoplanets. In this model, the planet-planet scattering mechanism led to the ejection and collision of some planets while leaving others in the orbits with high eccentricity. Their study stated that the eccentricity distribution of giant exoplanets with eccentricities above 0.3 in their sample is consistent with all of them being the result of planet-planet scattering (Carrera et al., 2019). Another research study in 2013 found some evidence that proto-hot Jupiters with high eccentricity are more common around metal-rich stars, which are known for having multiple gas giant planets (Dawson & Murray-Clay, 2013).

Although planet-planet scattering is altering the hot Jupiters semi-major access, it is unlikely that this mechanism can reduce the semi-major axis by a factor of 100 solely since in the

7

first step of the high-eccentricity tidal migration process, the orbital energy is conserved, and the hot Jupiter needs to eject about 100 planets to reduce its semi-major axis by a factor of 100.(Dawson & Johnson, 2018).

1.2.2.3.2   Secular interactions

This mechanism includes hypothetical additional bodies, with a focus on secular perturbations to explain the formation of hot Jupiters. Secular interactions take place over time scales that are long compared to observational time baselines, but it is still short compared to the age of the planetary system. Its time scale depends on the separation and mass of the companions involved (F. C. Adams & Laughlin, 2006). In the secular interactions mechanism, angular momentum between a widely-separated planet and stellar or non-stellar companion slowly exchange. Through secular interactions, a Jupiter-mass planet can gradually deposit its angular momentum into its companion in the system. This interaction might happen periodically (Kozai mechanism) or chaotically (secular chaos).

1.2.2.3.3   Kozai-Lidov Effect

The Kozai-Lidov effect states that a body under the presence of gravitational force can exchange periodic angular momentum with a distant massive companion. It is also possible that they exchange the orbital inclination and eccentricity as a periodic oscillation (Kozai, 1962; Naoz, 2016; Lidov, 1962). An outer body with a highly elliptical orbit in a coplanar planetary system can also experience Kozai-Lidov cycles. In 2012, Naoz et al. proposed that up to 100% of the orbital mis-alignments could be predicted by the models based on the dynamics of the Kozai mechanism. In 2003, a study by Wu & Murray proposed that Kozai migration is the only plausible explanation for the hot Jupiter existing in the HD 80606b planetary system. (Pont et al., 2009; Wu et al., 2007)

1.3   Purpose

In this work, I present a survey of direct imaging of hot Jupiter planetary systems. Out of 18 targets, 11 systems have published measurements of spin-orbit obliquity using the Rossiter-McLaughlin effect. The hot Jupiters in our sample are transiting planets from the Southern hemisphere. By focusing on this sample, I investigate the origin of their observed spin-orbit misalignments by searching for massive, distant companions in these systems. Our observations benefited from having stellar companion is inducing the spin-orbit misalignment of the hot Jupiter systems and to find any correlation between spin-orbit obliquity and presence of stellar companions.

CHAPTER II

OBSERVATIONS

Our observations were carried out with the VisAO (Instrument PI: Jared Males) and Clio (Instrument PI: Katie Morzinski) instruments on the MagAO system, which is an adaptive optics system on the 6.5 meter Magellan telescope located at Las Campanas Observatory, Chile. Clio is an infrared camera designed to detect low mass companion candidates at 3-5 μm (Morzinski et al., 2015). Clio has 2 pixel scales: 15.9 mas (milli-arcsecond) with a 16″×8″ Field of view (FOV) for the narrow camera and 27 mas with a 28″×14″ FOV for the wide camera. VisAO is a visible-light camera with limited diffraction (Males et al., 2014). Dr.Tinney and his team obtained observations on 8/4/2014 and 20/5/2015. The summary of the observations is available in Table 2.1. They used subarrays (1024 × 512 and 1024 × 300) pixels for the FOV on the narrow camera (0.0016" plate-scale) and the wide camera (0.0027" plate-scale) to avoid saturation and reduce the integration time on those targets. They didn't use any coronagraphs in these observations.

They used the Angular Differential Imaging technique in observation for a few targets in our sample. In the Angular Differential Imaging technique, astronomers gather a sequence of images with an altitude/azimuth telescope with the instrument rotator being turned off. This keeps the instrument and telescope optics aligned. By rotating back the sequence of images, using parallactic angle change, the image would be exposed, and the faint object close to a star would be detectable (see Figure 2.1). Vortex Image Processing package is the python package that I used

for reducing the data collected by this method (Gonzalez et al., 2017). This work is more focused on the analysis of the data collected by the Clio camera.

Table 2.1   Observation Summary Table

Target	NC	Observation Date	Filter	Plate Scale	Array	Int. time (ms)	Central Wavelength	Total Files
WASP-80	3	2014-04-08	H	0.027	1024×512	10000	1.65	233
		2014-04-08	Ks	0.027	1024×512	10000	2.15	80
		2014-04-08	Ks	0.027	1024×512	280	2.15	8
		2014-04-08	H	0.027	1024×512	280	1.65	23
HD 197286 / WASP-7	0	2014-04-08	Ks	0.016	1024×512	5000	2.15	360
		2014-04-08	Ks	0.016	1024×512	280	2.15	14
HAT-P-27	1	2014-04-08	Ks	0.016	1024×512	10000	2.15	132
		2014-04-08	Ks	0.016	1024×512	280	2.15	13
		2015-05-20	H	0.016	1024×512	30000	1.65	15
		2015-05-20	Ks	0.016	1024×512	5000	1.65	12
		2015-05-20	J	0.016	1024×512	30000	1.25	12
HAT-P-30	1	2014-04-08	Ks	0.016	1024×512	10000	2.15	59
		2014-04-08	Ks	0.016	1024×512	280	2.15	5
HD146389		2014-04-08	Ks	0.016	1024×512	5000	2.15	440
		2014-04-08	Ks	0.016	1024×512	280	2.15	44
HD 100623		2014-04-08	Ks	0.016	1024×300	164	2.15	44
		2014-04-08	Ks	0.016	1024×512	5000	2.15	642
		2014-04-08	Ks	0.016	1024×512	280	2.15	64
HD 74868		2014-04-08	Ks	0.016	1024×512	280	2.15	30
		2014-04-08	Ks	0.016	1024×512	164	2.15	40

Table 2.1 continued

Target	NC	Observation Date	Filter	Plate Scale	Array	Int. time (ms)	Central Wavelength	Total Fits Files
WASP-14	2	2014-04-08	Ks	0.016	1024×512	5000	2.15	176
		2014-04-08	Ks	0.016	1024×512	280	2.15	15
CD-27 9225	0	2014-04-08	KS	0.016	1024×512	10000	2.15	358
		2014-04-08	KS	0.016	1024×512	280	2.15	33
WASP-109	0	2015-05-20	H	0.016	1024×512	30000	1.65	49
WASP-20	1	2015-05-20	H	0.016	1024×512	15000	1.65	7
		2015-05-20	J	0.016	1024×512	5000	1.25	6
		2015-05-20	KS	0.016	1024×512	5000	2.15	6
WASP-5	0	2015-05-20	H	0.016	1024×512	30000	1.65	140
WASP-179	1	2015-05-20	H	0.016	1024×512	30000	1.65	85
HD160691	0	2015-05-20	H	0.016	1024×512	2000	1.65	55
HD106965	0	2015-05-20	H	0.016	1024×512	165	1.65	20
		2015-05-20	KS	0.016	1024×512	165	2.15	20
HATS-24	1	2015-05-20	H	0.016	1024×512	30000	1.65	67
HATS700-028	1	2015-05-20	H	0.016	1024×512	30000	1.65	76
HAT-P-41	1	2015-05-20	H	0.016	1024×512	30000	1.65	113

*Nc is the number of candidate companions.
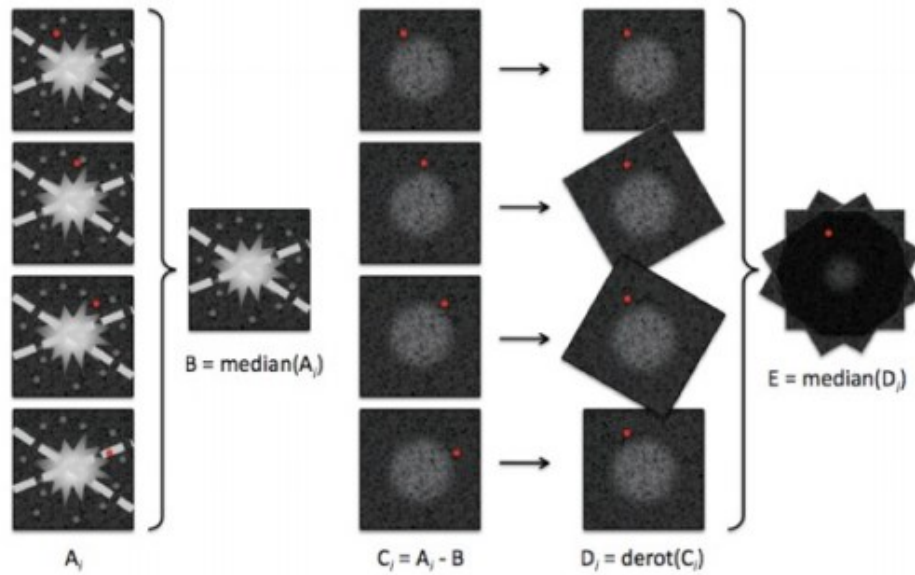
Figure 2.1   Angular   Differential   Imaging   technique.   Image   Credit   :   Taweewat
              Somboonpanyakul

2.2   Filters

Dr. Tinney and his team used H-band, J-band, and KS-band filters in these observations. In the 2014 data set, almost all the targets were observed using the Ks-band filter because the AO correction is superior at longer wavelengths. The wavelength range associated with each filter are shown in Figure 2.2, 2.3, 2.4. For target HAT-P-27 which have had a potential candidate at the time of observation, they repeated the observations in all three filters to obtain color information.
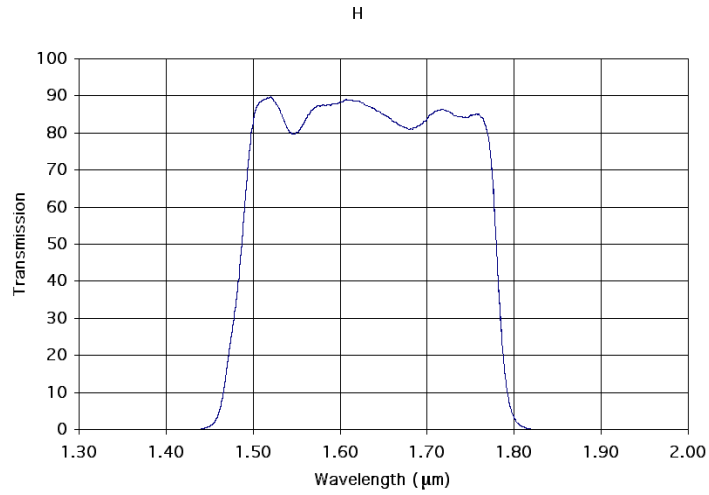
Figure 2.2   H band filter associated wavelength range (Image credit: Keck observatory website)
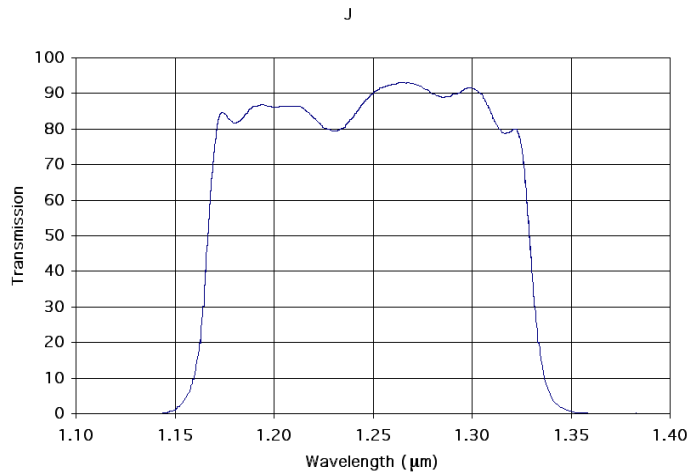
Figure 2.3   J band filter associated wavelength range (Image Credit: Keck observatory website)
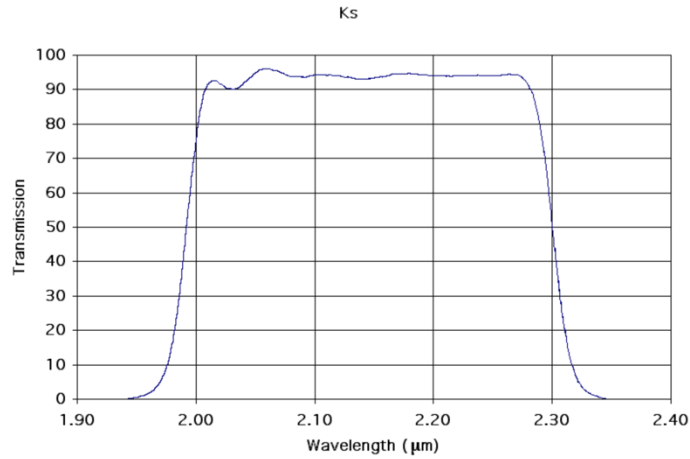
Figure 2.4   Ks band filter associated wavelength range (Image Credit: Keck observatory website)

2.3   Sample

Table 2.1 shows all the targets that we considered for this study. I summarized the stellar parameters and exoplanets properties of these systems in Table 2.2 and 2.3. We chose these targets based on their spin-orbit obliquity measurements. Ten targets out of these eighteen targets have known measured spin-orbit obliquity value (as listed in Table 2.4). Based on effective temperature (T_{eff})ragne of the targets in our sample (4145ºK - 6520ºK) almost all systems with known obliquity measurements in this study are solar type systems (see Figure 2.5 and 2.6).

Table 2.2   Sample Properties

Target	Sample	T eff (k)	Mass (M sun)	D (pc)	References
WASP-80	Misaligned	4145.0 +/- 100.0	0.58 +/- 0.05	60 +/- 20	T and D: (Amaury H. M. J. Triaud et al., 2013) M: (Amaury H. M. J. Triaud et al., 2015)
HAT-P-27	Misaligned	5300.0 +/- 90.0	0.945 +/-0.050	204+/- 14	T M and D: (Béky et al., 2011)
HD 197286 /WASP-7	Misaligned	6400.0 +/-100.0	1.276 +/- 0.06	140.0 +/- 15.0	T and M: (Southworth et al., 2011) D:(Hellier et al., 2008)
HAT-P-30	Misaligned	6250.0 +/- 100.0	1.18 +/- 0.03	193.0 +/- 8.0	T and M: (Enoch et al, 2011) D: (J. A. Johnson et al., 2011)
HD146389	Misaligned	6150.0 +/- 80.0	1.216 +/-0.041	110.0 +/- 20.0	T M and D: (Barros et al., 2011)
HD 100623	None	5189	0.81	9.543	T and M: (Turnbull, 2015) D: (Gaia Collaboration, 2018)
HD 74868	None	None	None	36.462	D: (Gaia Collaboration, 2018)
GJ 510	None	3630	0.43	15.388	T: (Turnbull, 2015) D: (Gaia Collaboration, 2018)

Table 2.2 continued

Target	Sample	T eff (k)	M (M sun)	D (pc)	Ref
WASP-14	Misaligned	6462 +/- 75	1.62+/-0.39	160.0 +/- 20.0	T: (Johnson et al., 2009) M: (Stassun et al., 2017) D: (Gaia Collaboration, 2018): (Turnbull, 2015)
WASP-109	Misaligned	6520 +/- 140	1.203+/- 0.09	330.0 +/- 30.0	T: (Addison et al., 2018) M and D: (Anderson et al., 2014)
WASP-20	Misaligned	5940+/-100	1.200+/- 0.041	210.0 +/- 20.0	T D and M: (Anderson et al., 2015)
WASP-5	Misaligned	5770 +/- 65	0.96+0.13-0.09	311.882+/- 3.411	T: (A. H. M. J. Triaud et al., 2010) M and D: (Gillon et al., 2009)
WASP-179	Misaligned	6450 +/- 50	1.64 +0.19-0.22	360.3 +8.3-7.8	T: (Anderson et al., 2018) M and D: (Raynard et al., 2018)
HD160691	None	5700.0 +/- 100.0	1.08 +/- 0.05	15.3	T M and D: (Pepe et al., 2007b) M and D: (Gillon et al., 2009)
HATS24	None	6125+/-94	1.070+0.032-0.046	510+/- 15	T M and D: (Oliveira et al., 2019)
HATS700-028	None	None	None	552.303	D :(Gaia Collaboration, 2018)
HAT-P-41	Misaligned	6390+/-100	2.56+/- 1.90	351.634+/- 4.527	T: (M. C. Johnson et al., 2017b) M and D: (Stassun et al., 2017)

Table 2.3   Planet Properties

Hot Jupiter	Period	Eccentricity	R (R Jup)	Mass (M Jup)	Semi-major axis	Reference
WASP-14 b	2.24375	0.09	1.38 +/- 0.08	8.840 +/- 1.400	0.0358	R M P E: (Stassun et al., 2017) T: (Raetz et al., 2015) SMA: (Bonomo et al., 2017)
WASP-80 b	3.067852	0.002	0.999	0.538	0.0344	R M P:(Stassun et al., 2017) E and SMA: (Amaury H. M. J. Triaud et al., 2015a)
WASP-7 b	4.954641	0.00	1.330 +/- 0.093	0.960+/- 0.130	0.0617	R M P and SMA: (Southworth et al., 2011, p. 7) E: (Stassun et al., 2017)
WASP-38 b	6.87188	0.03	1.23 +/- 0.06	3.44 +/- 0.36	0.07584	R M P E and T: (Stassun et al., 2017) SMA:(Bonomo et al., 2017)
HAT-P-30b	2.8106	0.04 +/- 0.02	1.44 +/- 0.15	0.830 +/- 0.180	0.0419	R M P E: (Stassun et al., 2017) SMA:(Bonomo et al., 2017)
HAT-P-27b	3.039577	0.00	1.02	0.62 +/- 0.03	0.04	R M P E and SMA: (Brown et al., 2012)
WASP-109 b	3.319023	0.00	1.443	0.91 +/- 0.13	0.0463	ALL: (Anderson et al., 2014)

Table 2.3 continued

Hot Jupiter	Period	Eccentricity	R (R Jup)	Mass (M Jup)	Semi-major axis	Ref
WASP-20 b	4.8996	0.00	1.462+/-0.059	0.311+/-0.017	0.06	ALL: (Anderson et al., 2015)
WASP-5 b	1.6284	0.038+0.026 -0.018	1.087	1.58	0.0267	R M P and E: (Anderson et al., 2015) SMA: (Gillon et al., 2009)
NGTS2 b/ WASP-179b	4.5111	0.00	1.595	0.74+0.13-0.12	0.063	ALL: (Raynard et al., 2018)
HD160691b	643.25 +/- 0.9	0.128 +/- 0.017	None	1.676	1.50 +/-0.02	P E and M: (Pepe et al., 2007b) SMA:(Pepe et al., 2007)
HAT-P-41 b	2.6940	0.00	2.05+/-0.50	1.19+/-0.60	0.04258	R M P and E: (Stassun et al., 2017) SMA: (Bonomo et al., 2017)
HATS24 b	1.3484	0.00	1.395+/-0.057	2.26+/-0.17	0.0238	ALL: (Oliveira et al., 2019)

Table 2.4   Spin-Orbit Obliquity Table

Star Name	Lambda	Reference
WASP 80	$-14.0^{+14.0}_{-14.0}$	(Triaud et al., 2015b)
WASP 7	$86.0^{+6.0}_{-6.0}$	(Albrecht et al., 2012)
WASP-38	$7.5^{+4.7}_{-6.1}$	(Brown et al., 2012)
HAT-P-30	73.5^{+9}_{-9}	(Johnson et al., 2011)
HAT-P-27	$24.2^{+44.5}_{-76.0}$	(Brown et al., 2012)
WASP14	$33.1^{+7.4}_{-7.4}$	(Johnson et al., 2009)
WASP109	$99.0^{+10.0}_{-9.0}$	(Addison et al., 2018)
WASP20	$12.7^{+4.72}_{-4.2}$	(Anderson et al., 2015)
WASP-5	$12.1^{+10.0}_{-8.0}$	(Triaud et al., 2010)
HAT-P-41	$-22.1^{+6.0}_{-0.8}$	(Johnson et al., 2017b)
NGTS2	$-11.3^{+4.8}_{-4.8}$	(Anderson et al., 2018)
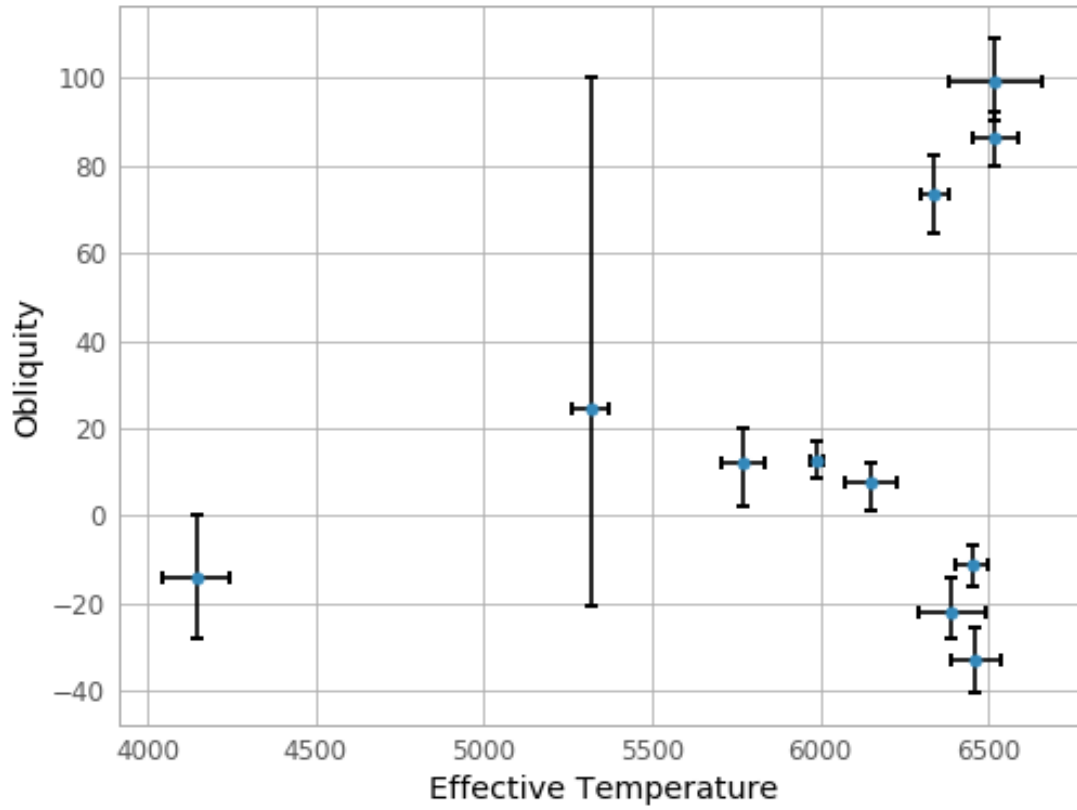
Figure 2.5   Spin-Orbit Obliquity versus Effective Temperature of all targets considered in this study.
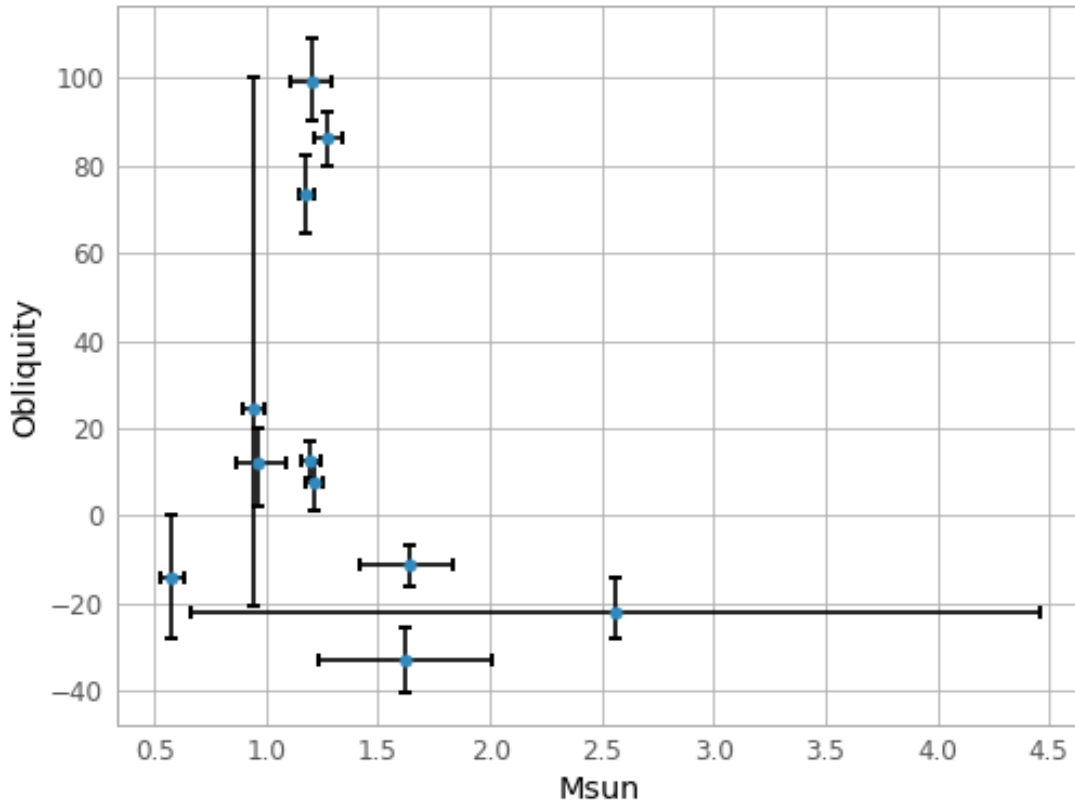
Figure 2.6   Spin-Orbit Obliquity versus stellar Mass for all targets considered in this study.

2.4   Data Reduction

The necessary steps in data reduction for each telescope and each instrument might be different. Therefore, data collected using VisAO and Clio must be treated differently since these two cameras generate two completely different data sets in visible-light and infrared light. Here, I focus on describing the data reduction for infrared data using Clio on the MagAO system. During this work, I have made a Jupyter Notebook as a guide to data reduction of data collected using the Clio instrument.

For reducing Clio data, we need to take several steps, including: Linearity correction, subtracting Darks and dividing by Flats, bad pixels correction, sky subtraction via nod pairs,

22

centroiding the target and trimming the image, rotating the images. I will review each step in this section.

2.4.1   Linearity Correction

Linearity correction is a correction to the raw pixel count. Therefore, it must be applied to the raw pixels as the first step of the data reduction for Clio. Linearity determined by subtracting true count (y)(true count is the count rate which gives a linear relationship with the integration time of each fits file) from measured count (x) and normalize it by the true count(Morzinski, 2014; Morzinski et al., 2015). Whenever we need to do differential intensity measurements, Correcting the non-linearities in the images becomes very important. This correction applies on any pixel that has a value (x) more than 27000.The correction is part of the code that we used for Mag-AO Clio data. The 3rd order polynomial equation used is

$$y = A + Bx + Cx^2 + Dx^3 \qquad\qquad (2.1)$$

Where y is the true count and x is the measured count, where A=112.575, B=1.00273, C=-1.40776$\times 10^{-06}$, and D=4.59015$\times 10^{-11}$. The x value must be more than 27000. For the images with coadds, we had to divide the count by the number of the coadds before applying the linearity correction(Morzinski et al., 2015).

The linearity correction for each pixel would not necessarily lower the value of value pixel to a value of less than 27000. It is just going to smooth the whole image. (Morzinski, 2014; Morzinski et al., 2015)

2.4.2   Subtracting Darks and Dividing by Flats

Dark frames are calibration images which are temperature and integration time depended. During the observation, camera's temperature cause some thermal noises which

effect the images. We calibrate the noise caused by the instrument using dark frames. Flat frames show the imperfections in the light path in the images which needs to be obtained in each filter. We calibrated the images from our observation using the dome flat fields and dark frames provided by the instrument specialist and the Clio instrument website. The integration time of the dark frames and the wavelength band of the flat files should match the science data.

2.4.3 Bad Pixel Correction

Unlike Bad pixel or dead pixel are transistors that are damaged and dead, which cause black, white or colored dots in the image. Unlike visible imaging instruments, the technology in infrared cameras are not good enough to neglect the bad pixel correction. The Clio camera has a bad pixel mask which astronomer can use for fixing the bad pixels in the images. Most infrared instruments have their own bad pixel mask, which gets updated by the instrument specialists.

In bad pixel reduction, first we determine the median and standard deviation of each cluster of 5 pixels in each image. There is a bad pixel mask available for the Clio instrument which was provided by the instrument specialist. The mask is a value combination of 0 and 1 which means any pixel with value 1 is a bad pixel and needs to be replaced with the median of its surrounding pixels.

2.4.4 Sky subtraction via nod pairs

All the Clio images, are nodded from side to side to make sure a star is always on the camera chip. That's why we need to do nod paring for the Clio data. They are either ABBA or AB. Since the position of the star in each set of images changes in order to do the nod pairing, the sky subtraction is a key step to separate the background sky and the target.

2.4.5   Centroiding the target and trimming the image

In order to detect the potential faint companions, of a star the main targets in most of our images are saturated. There is a centroid Python package that has been written for Clio data analysis, which allows for a precise estimate of the position of a saturated star. Saturated stars in images are caused by long integration time for bright stars, basically only a limited number of electrons can be stored in each pixel of the image and if the electron number pass the limit the pixel would be overflowed and saturated. All the images were trimmed to squares of (300$\times$300) pixels except for two targets. Hat-P-30 and WASP 14 are the only targets with distant companion candidates, where we had to trim them differently to make sure the companion is in the final image.

2.4.6   Rotating the Images

We needed to rotate all the final science images with respect to the instrument angle "NorthClio" using the direction equation:

$$DEROTClio =\ ROTOFF - 180\ +\ NorthClio \tag{2.2}$$

In equation (2.1), DEROTClio is the derotation angle, ROTOFF is the rotation angle of each image from North-East direction, and NorthClio is the instrument angle. The value of NorthClio is -1.797(340). All CLIO images have to be rotated counter- clockwise (Morzinski et al., 2015).

CHAPTER III

DATA ANALISYS

This chapter provides the information regarding how we analyzed this data and basic information and an explanation of the data sample and its properties. During this work, we collected and analyzed the data for 18 star systems, and we identified companion candidates around 8 of our targets. We summarize the sample parameters and the planet properties for all observed targets in Table 2.2 and 2.3.

Our companion candidates are identified by visual inspection. However, due to the small field of view of VisAO, we were not able to observe all the companion candidates that we detected in the Clio. We processed the images as I mentioned in the Data Reduction section (2.2).

We measured the flux ratio (the ratio of the intensity of light emitted by the host star and the candidate companion) and on-sky separation for each target with the detected companion candidate. By integrating the point spread function (PSF) over a circular aperture for the reference star and all the targets, we could get the flux ratio for each target. Using the flux ratio of the reference star, we performed photometry on all the targets with a companion candidate. Our reference star for this data collection is HD 106965, which is an A0 type star with a distance of 273.35 pc away from the Sun.

In order to get the on-sky separation and position angle (between the host star and the candidate) for each target, I performed an astrometric correction on each target. These astrometric corrections include uncertainties in the plate-scale of the instrument and orientation of the CLIO.

I estimated the measurement error for separation and position angle as the standard error on the mean value of all calibrated frames. In this chapter, we can report the estimated flux ratio between the host star and the candidate/s as a magnitude difference in each filter.

Using the host star distance, our measured on-sky separations, I could calculate the projected spatial separations. WASP-20 is our only target that not have a measured parallax therefore I used a spectroscopic distance for astrometric corrections.

3.1   Notes on the Samples

We found 11 stellar companion candidates around the targets that we observed of which 5 are reported for the first time. In this part, I discuss each stellar system individually and categorize them if they have a confirmed bound companion. Our analysis could validate or confirm 6 as gravitationally bound companions to the host star in these systems. I also discuss any previous observations that reported about our targets by other studies.

3.1.1   HAT-P-27 (WASP-40)

HAT-P-27 is a G8 type star with a mass of 0.945+/- 0.035 M_{Sun}. HAT-P-27 hosts a transiting gas giant planet with a mass of 0.62 +/- 0.03 M_{Jup}, , an orbital semi-major axis of 0.04 AU, and a period of 3.0396 days (Béky et al., 2011). HAT-P-27b is a hot Jupiter with misalignment in its spin-orbit because this planet has an eccentricity of 0.078 ± 0.047 and a spin-orbit alignment angle, λ, of $24.2^{+44.5}_{-76.0}$ (Béky et al., 2011; Brown et al., 2012).   In 2015, Wöllert & Brandner announced a close companion with a separation of 0.656 +/- 0.002 arc-second around this target. Later in 2016, Ngo et al. confirmed that this companion with the same separation of 0.656 +/- 0.002 arc-second is physically bound to the system (Ngo et al., 2016; Wöllert & Brandner, 2015).

We also observed this companion with separations of 0.655 +/- 0.008 arc-second and 0.665 +/- 0.004 arc-second in 2014 and 2015 respectively, and the delta magnitude in H filter is ΔH = 7.05 (see Figure 3.1) in Clio images. Figure 3.3 presents the final images of HAT-P-27 from VisAO. The companion is also visible in this image with separation of 0.669 arc-second or 134.02 AU (The VisAO images are reduced and processed by Claire Geneser). As Figure 3.2 shows, we can validate the Ngo et al. (2016) companion confirmation.
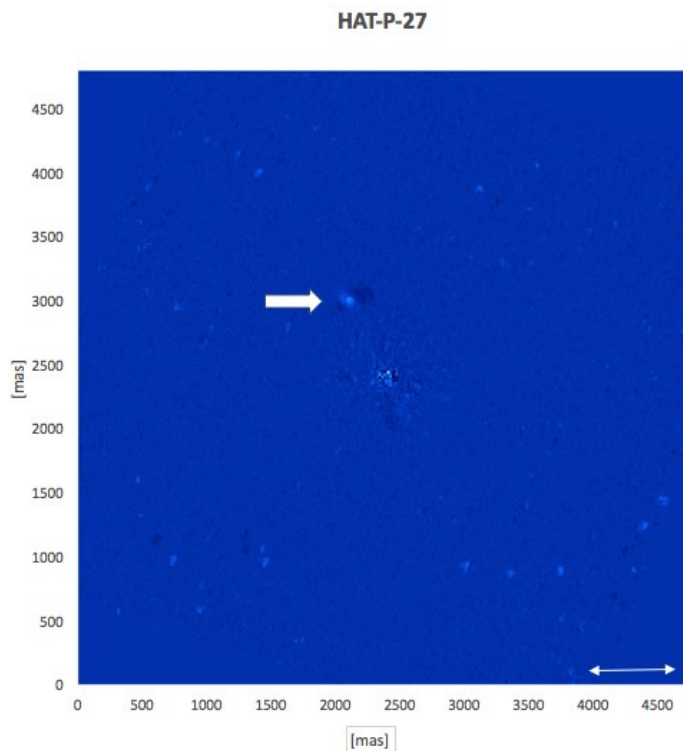
Figure 3.1   HAT-P-27. Image from Clio; The confirmed companion is above the main star. With a separation of 0.656 arc-second, the companion is 133AU away from the host star.
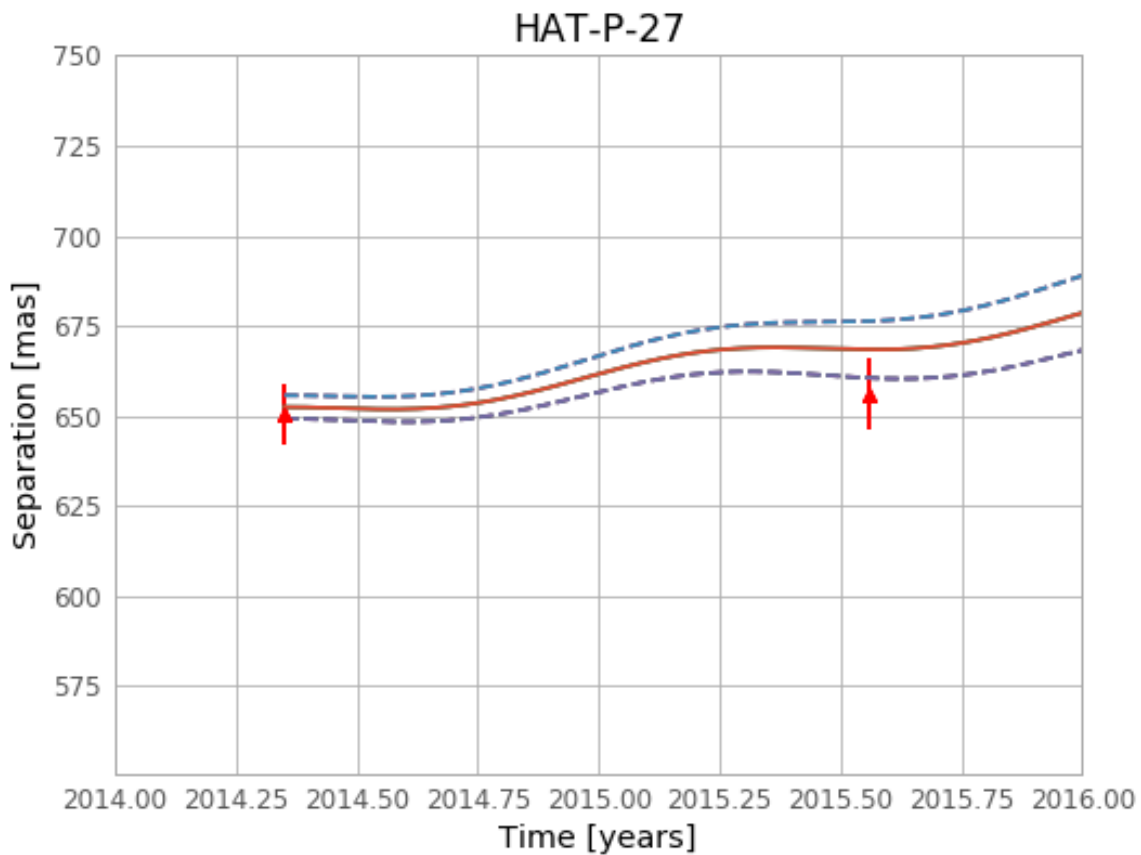
Figure 3.2 The image shows that the separation of the companion around HAT-P-27 did not significantly change in one year. The wavy lines in the Figure stands for the proper motion of the star and its error bars
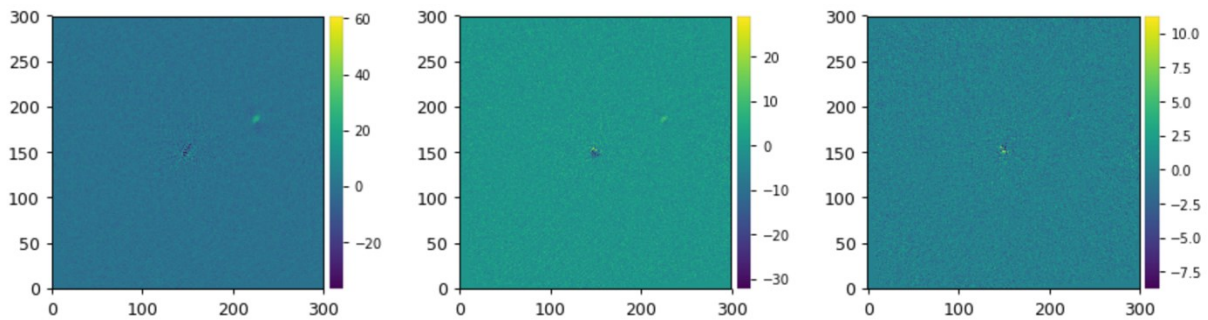
Figure 3.3 HAT-P-27; Image from VisAO; field of view is 2.4 x 2.4 arc-second; an object is located up and right of the main star. With a parallax of 4.9922, this object is at an estimate separation of 0.669" or 134.02 AU. (Image Credit: Claire Geneser)

3.1.2   HATS776-001 (HATS-24)

(Bento et al., 2017) reported a transiting gas giant planet around HATS-24 with a mass of 2.44 +/- 0.18 M_{Jup}, an orbital semi-major axis of 0.025AU, and a period of 1.348 days. Planet HATS-24b has an eccentricity of $0.24^{+0.0}_{-24.0}$. There is no obliquity measurement available for this target since the planet had been discovered in 2016. Therefore, we cannot count this system as a misaligned system. We found a companion candidate with a separation of 0.4+/- 0.9 arc-second and position angle (PA) of -37.757+/- 0.013 degrees around this target. This system needs a second epoch of data for common proper motion follow up to check in the candidate is bound to the system.

3.1.3   HD 197286 (WASP7)

HD 197286 is a F5V type star with a mass of 1.276 +/- 0.006 M_{Sun}. HD 197286 hosts a transiting gas giant planet with a mass of 0.96 +/- 0.13 M_{Jup}, an orbital semi-major axis of 0.061 AU, and a period of 4.954 days (Southworth et al., 2011). WASP-7b is a hot Jupiter with misalignment in its spin-orbit because this planet has an eccentricity of $0.034^{+0.045}_{-0.024}$ and a spin-orbit alignment angle, λ, of 86 +/- 6 (Albrecht et al., 2012; Knutson et al., 2014). In 2016, Evans et al. reported a companion candidate with a separation of 4.414+/- 0.011 arc-second around this target (D. F. Evans et al., 2016). A recent study by Bohn et al. (2020) showed that WASP-7 with a separation of 4.474 +/- 0.007 is a background object (Bohn et al., 2020). We were not able to see this background object in our observation.

3.1.4   WASP-20

WASP-20 hosts a transiting gas giant planet with a mass of 0.311+/- 0.017 M_{Jup}, an orbital semi-major axis of 0.06 AU, and a period of 4.8996 days. WASP-20b belongs to a misaligned

spin-orbit system with a λ of 12.7+/- 4. 2 and eccentricity of 0.0(Anderson et al., 2015, p. 20). In

2016, Evans et al. reported a close companion around WASP-20(D. Evans et al., 2016). Recently,

Bohn et al. in 2020 re-analyzed the same data and published the separation of 0.259+/- 0.003 for

this target (Bohn et al., 2020). Although our data shows the close-in companion around WASP-20

with a separation of 0.256 +/- 0.002 arc-second and position angle of 214.824+/- 0.343 degrees,

we need a follow up observation on this target because the error bars of proper motion of the star

are too large (see figure 3.4 and 3.5).
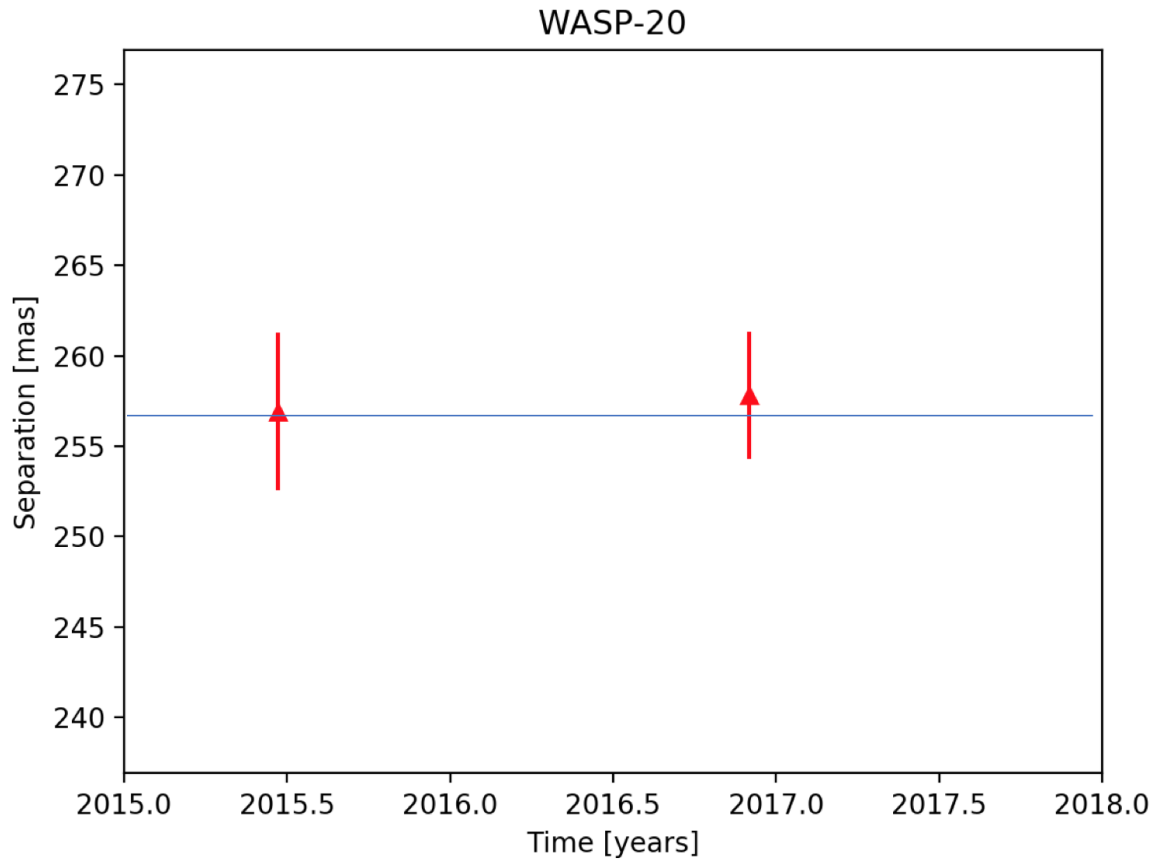
Figure 3.4   The figure is Separation vs. Time. We generated the graph using the separation
that is reported by Evan et al. (2016) and our observation in 2015.
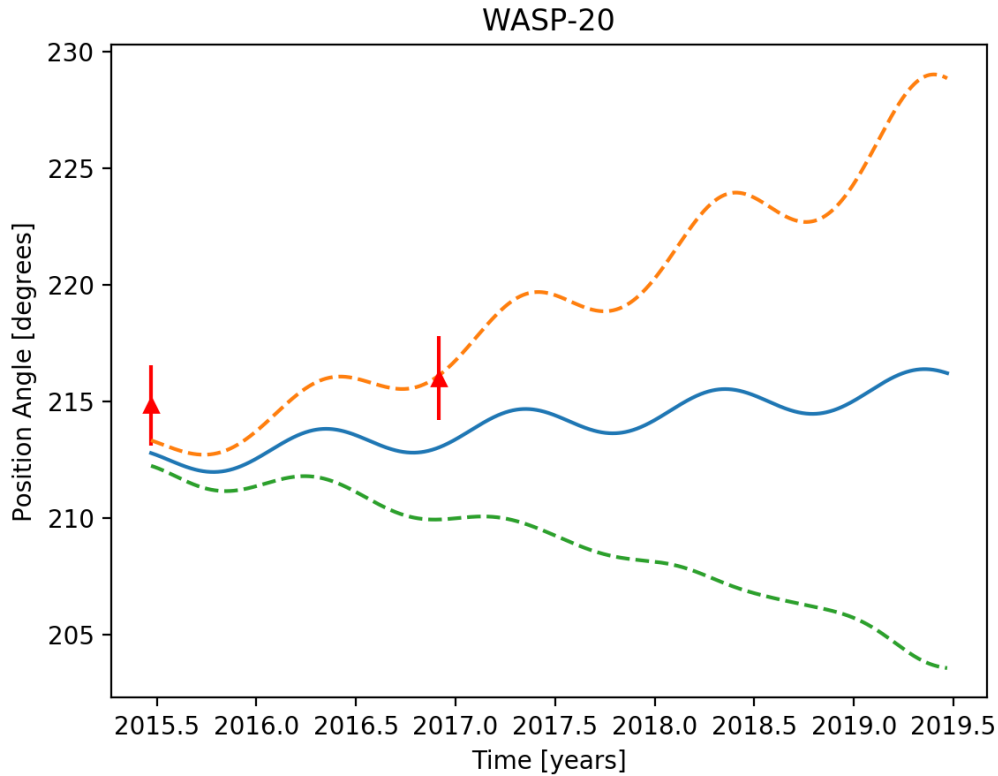
Figure 3.5   WASP-20; Position angle versus Time graph; The second observation data point is from Evan et al. (2016). The wavy lines in the image show the proper motion of the star and its error bars.

3.1.5   HAT-P-41

In 2012, Hartman et al. report the discovery of a hot Jupiter around HAT-P-41. HAT-P-41b is a gas giant with a mass of 1.1960 M_{Jup}, an orbital semi-major axis of 0.043 AU, and a period of 2.694 days. HAT-P-41b belongs to a misaligned spin-orbit system with a λ of $-22.1^{+6.0}_{-0.8}$ and eccentricity of 0.0 (Johnson et al., 2017a; Stassun et al., 2017). They also detected a companion candidate south of this star. Wöllert et al., Wöllert & Brandner (2015), Eavan et al. (2016), and Ngo et al. (2016) also detected this candidate in the same position with the separation angle of 3.615 +/- 0.002 arc-second and the position angle of 184.10 +/- 0.03 degree (D. F. Evans et al., 2016; Ngo et al., 2016; Wöllert & Brandner, 2015). Recently, Bohn et al. in 2020 reported that

33

their team detected the same companion with a separation of 3.621 +/- 0.004 and a position angle of 183.9 +/- 0.1 degrees. The mass of this companion is estimated to be $0.71^{+0.06}_{-0.05}$ M_{Jup}(Bohn et al., 2020). Our data were collected in 2015, and we could detect the same target with a separation of 3.64 +/- 0.17 arc-second. We validate that HAT-P-41B is a bound stellar companion in the HAT-P-41 system.

3.1.6   WASP-80

WASP-80 is a K7V type star with a mass of 0.58 +/- 0.05 M_{Sun}. WASP-80 is a planetary system with a transiting gas giant planet with a mass of 0.554 M_{Jup} an orbital semi-major axis of 0.0349 AU, and a period of 3.068 days (Triaud et al., 2013). WASP-80b is a hot Jupiter with a spin-orbit misalignment where the planet has an eccentricity of $0.07^{+0.0}_{-0.07}$ and a spin-orbit alignment angle, λ, of -14 ± 14 (Triaud et al., 2013, 2015b). Bohn et al. 2020 report the detection of a companion candidate around this target with separation of 2.132 +/- 0.010 arc-second and a position angle of 275.5 +/- 0.3 arc-second. We could detect the same companion with the separation of 2.662 +/- 0.009 and the position angle of 8.004 +/- 0.045 degrees (Figure 3.6). Using the published results of Bohn et al. from data that was collected on 2017-06-22, we can confirm that a companion is a background object since it moved with the proper motion of the star (see Figure 3.7). Our analysis shows there are another two candidate companions around this target with separations of 3.965 +/- 0.013, 3.964 +/- 0.013 arc-second and position angles of -44.157 +/- 0.045, -40.456 +/- 0.040 degrees, respectively, in Ks and H filters. These two candidates have their own separation of 0.016 arc-sec or 0.79 AU. Our initial estimate shows the magnitude of the individual components of about 15.5 magnitudes at 1.65 microns or ΔH = 7.15 for the double companion candidates compared to the host star. Figure 3.8 presents the processed images from

34

VisAO. Due to a small field of view, we could not see these two candidates in the VisAO images.

These double companion candidates are most likely a very close M dwarf binary. We believe Bohn

et al. could not detect the other two companions due to the limitation of their field of view

.
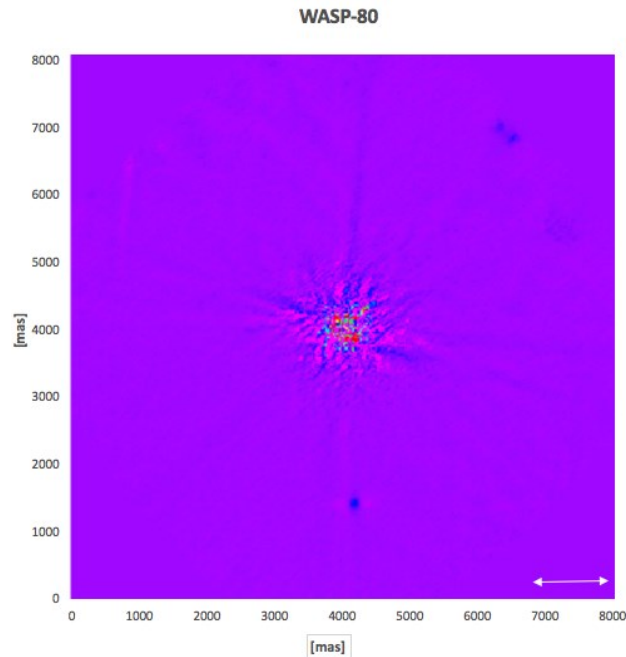
Figure 3.6   WASP-80; ADI image from the Clio; There are three candidate companions in the image. There are two not confirmed companions upper right which lies at a separation of 3.965 arc-sec (237.89AU) from the host star and has its own separation of 0.016" or 0.79 AU if we assume it is at the same distance as the host star. There is one companion below the main star with separation of 2.662 arc-sec (159.72 AU) from the host star. Length of the arrow in the image shows one arc-second.
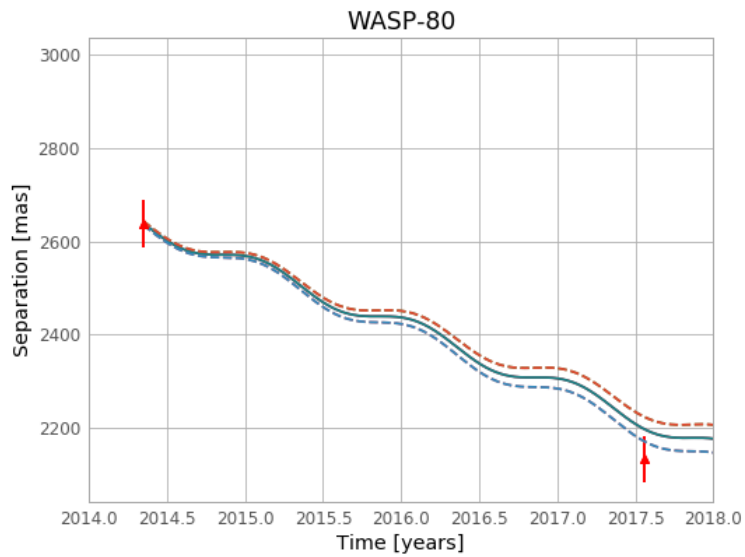
Figure 3.7   WASP-80; Separation versus Time graph; The second observation data point is from Bohn et al. (2020), and the first data point is from our observation in 2014. The image shows that the candidate is a background object. The wavy lines in the image show the proper motion of the star and its error bars.
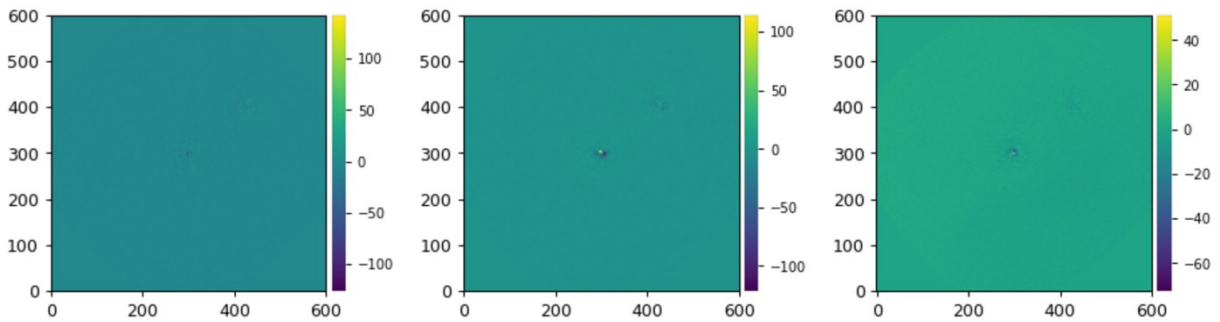
Figure 3.8   VisAO processed image of WASP 80. Field of view 4.8 x 4.8 arc-second; the companion is located up and right of the main star (Credit: Claire Geneser)

36

3.1.7   WASP-109

WASP-109 hosts a transiting gas giant planet with a mass of 0.91 +/- 0.13 M_{Jup}, an orbital semi-major axis of 0.0463 AU, and a period of 4.8996 days. WASP-109b belongs to a highly-misaligned system with a λ of $99^{+10.0}_{-9.0}$ and eccentricity of 0.0 (Addison et al., 2018; Anderson et al., 2014). We could not detect any companion around this target.

3.1.8   WASP-5

WASP-80 is a G4V type star with a mass of 1.03 M_{Sun}. This star hosts a transiting gas giant planet with a mass of 1.59 M_{Jup}, an orbital semi-major axis of 0.027 AU, and a period of 1.628 days (Bonomo et al., 2017). WASP-5b is a hot Jupiter with a spin-orbit misalignment characterized by eccentricity of 0.0 and a spin-orbit alignment angle, λ, of $12.1^{+10.0}_{-8.0}$ (Triaud et al., 2010). We could not detect any companion around this target.

3.1.9   HAT-P-30

HAT-P-30 hosts a transiting gas giant planet with a mass of 0.83 M_{Jup}, an orbital semi-major axis of 0.0419 AU, and a period of 2.81days (Bonomo et al., 2017; Stassun et al., 2017). HAT-P-30b was discovered independently by both the Wide-Angle Search for Planets (WASP) survey and the Hungarian-made Automated Telescope (HAT) in 2011(Enoch et al., 2011; J. A. Johnson et al., 2011). This planet belongs to a misaligned spin-orbit system with a λ of 73.5 +/- 9.0 and eccentricity of 0.04 +/- 0.02 (Johnson et al., 2011; Stassun et al., 2017). Adams et al. (2013) reported the detection of a companion around HAT-P-30 which later was confirmed by Ngo et al. (2015) with separations of 3835.1 +/- 1.7 mas and 3836.6 +/- 1.7 (mas) collected in 2012 and 2015 (E. R. Adams et al., 2013; Ngo et al., 2015). Ngo et al. (2015) confirmed that HAT-P-30 B is gravitationally bound to the system. We have only one epoch of observation from this target in

2014, and our analysis shows a companion with a separation of 3.86 +/- 0.05 arc-second and PA of -69.4 +/- 1.3 degrees, which agrees with the previous data published on this target (see Figure 3.9). We can validate the confirmation that HAT-P-30 B has a bound companion.
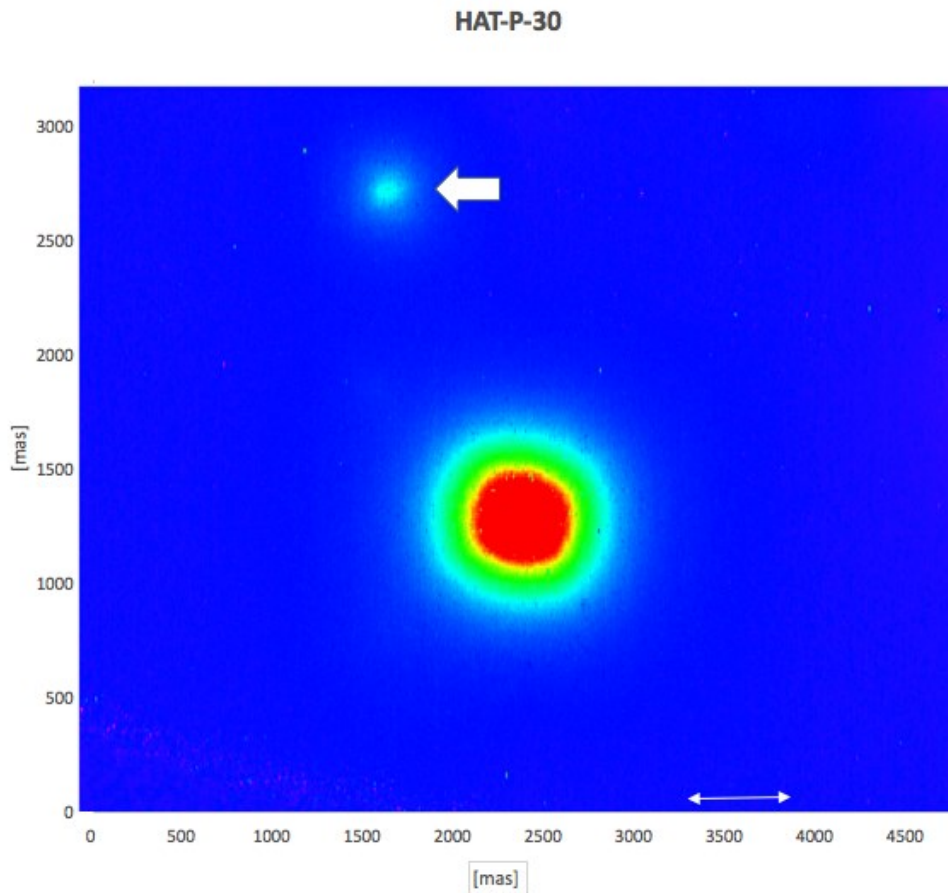
Figure 3.9   HAT-P-30, Image from Clio; The confirmed companion is above the main star with a separation of 3.86 +/- 0.05 arc-second. Length of arrow in the Figure shows one arc-second.

3.1.10   HD160691(μ Arae)

HD 160691 is a main sequence G3 IV-V type star which hosts a complex multi-planetary system with four confirmed exoplanets. μ Arae b is a hot Jupiter with a mass of $1.676 M_{Jup} \sin(i)$, an orbital semi-major axis of 1.50 +/- 0.02 AU, and a period of 9.63 days. μ Arae c is a hot Neptune with misalignment in its spin-orbit with an eccentricity of 0.172 +/- 0.040 and a λ of 17.6 +/- 0.4 (Pepe et al., 2007). Our data does not show any companion around this target.

3.1.11   WASP-179 (KS25C013712/NGTS-2)

WASP-179 (a.k.a NGTS-2) is a F5 V type star with a mass of $1.64 \, {}^{+\,0.19}_{-0.22} \, M_{Sun}$. This star hosts a gas giant exoplanet named WASP-179b (NGTS-2b) with a mass of $0.74 \, {}^{+\,0.13}_{-0.12} \, M_{Jup}$, an orbital semi-major axis of 0.063 AU, and a period of 4.51 days. NGTS-2b is slightly misaligned in its spin-orbit axis with a λ of −19 +/- 6 degrees and an eccentricity of 0.0 (Addison et al., 2018; Anderson et al., 2018). We found a companion candidate with separation of 0.648 +/- 0.014 and position angle of -82.5 +/- 8.0 around this target. We have only one observation epoch of WASP-179 and we need a follow up observation on this target to be able to confirm if this companion candidate is bound to the system.

3.1.12   WASP-14 (BD+22 2716)

WASP-14 A is F5 V type star with a mass of 1.62 +/- 0.39 M_{Sun}. This star hosts WASP-14b, a hot giant gas planet, with a mass of 8.540 M_{Jup}, an orbital semi-major axis of 0.0355 AU, and a period of 2.24 days (Blecic et al., 2013). WASP-14b belongs to a slightly misaligned system with a λ of $−14 \, {}^{+22}_{-13}$ and eccentricity of 0.087 +/- 0.002 (Blecic et al., 2013; Joshi et al., 2009). There are two known companion around WASP-14 A, where one companion, WASP-14 B, was confirmed by Ngo et al. (2015) and Wöllert & Brandner (2015). WASP-14 B is a stellar bound

companion with a separation of 1.45 arc-second (Ngo et al., 2015; Wöllert & Brandner, 2015). In 2019, Fontanive et al. reported the detection of a second companion for this target with a separation of 11.5397 +/- 0.0001 arc-second and position angle of 4.5827 +/- 0.0003 degrees which projects a wide separation of 1900 AU from WASP-14 A. They also characterized WASP-14 C to be a K5 dwarf with a mass of 0.28 M_{Sun}.(Fontanive et al., 2019) We validate stellar companion WASP-14 B with separation of 1.451 +/- 0.007 arc-second. We could not see the second companion in our observation.

3.1.13   HD 146389 (WASP-38)

HD 146389 (WASP-38) is the hosts a transiting gas giant planet with a mass of 3.44 +/- 0.36 M_{Jup}, an orbital semi-major axis of 0.076 AU, and a period of 6.871 days. HD 146389b belongs to a misaligned system with a λ of $7.5^{+4.7}_{-6.1}$ and eccentricity of 0.03 (Stassun et al., 2017).Our observations did not show any companion around this target.

3.1.14   HATS700-028

This target is only available on Gaia catalog with a 552.3 pc away from the Sun (Gaia Collaboration, 2018). HATS700-028 doesn't have any known hot Jupiter. There is no previous studies or observations on this target. Our observation shows there is a candidate companion with separation of 0.39+/- 0.11 arc-second around this target (see Figure 3.10). We need a follow up observation to be able to confirm this candidate as a bound companion around HATS700-028.
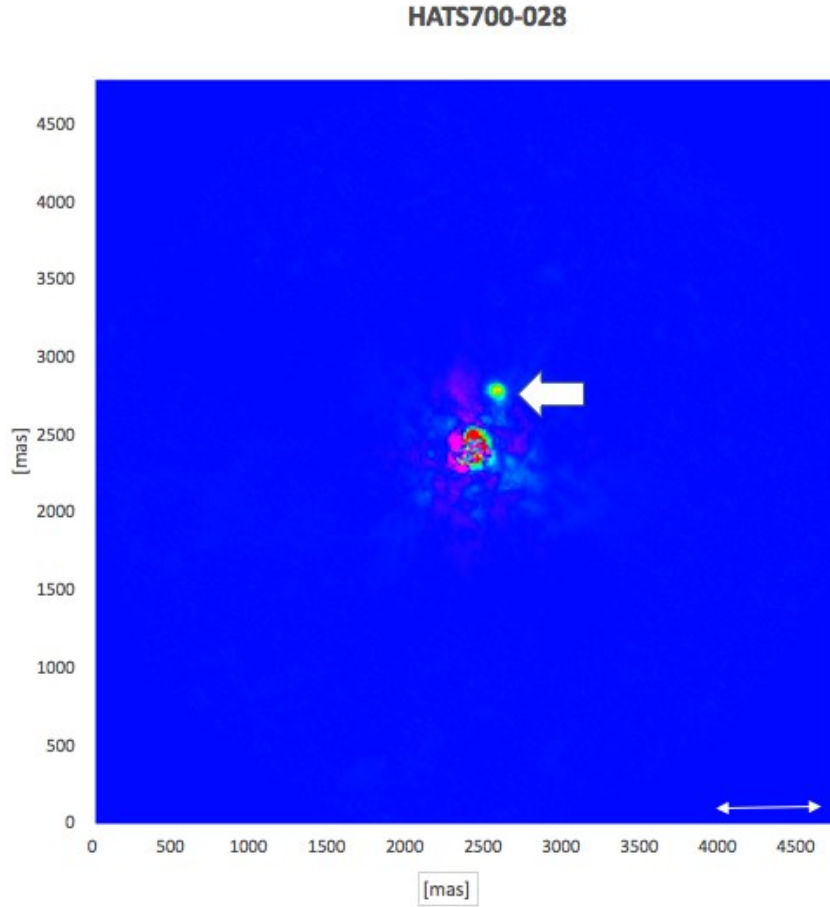
Figure 3.10   HATS700-028. Image from Clio; The not confirmed companion is shown on the ADI image of the target with separation of 0.39+/- 0.11 arc-second. Length of the arrow in the image shows one arc-second.

3.1.15   HD 100623

HD 100623 is a K0V C type star with a mass of $0.81\ M_{Sun}$ with a distance of 9.543 pc from the Sun (Turnbull, 2015; Gaia Collaboration, 2018). This system does not have a known hot Jupiter. Our observations did not show any companion around this target.

3.1.16 HD 74868

HD 74868 is a F9III-IV C type star with a distance of 36.462 pc from the Sun (Gaia Collaboration, 2018). This system does not have a known hot Jupiter. Our observations did not show any companion around this target.

3.1.17 GJ 510

GJ 510 is a M1 D type star with a mass of 0.43 M_{Sun} and a distance of 15.388 pc from the Sun (Turnbull, 2015; Gaia Collaboration, 2018). This system does not have a known hot Jupiter. Our observations did not show any companion around this target.

Table 3.1   Candidates Companion Separation Table

Target Name	*Nc	Separation (arc-second)	Separation(AU)	Candidate Status
WASP-80	3	2.662 +/- 0.009 3.965+/- 0.013 3.964+/-0.013	159.72 +/- 53.24 237.89 +/- 79.30 237.84 +/- 79.28	Not confirmed
HAT-P-27	1	0.665 +/- 0.004	133.8 +/- 9.0	Confirmed
HAT-P-30	1	3.86 +/- 0.05	744.9 +/- 32.0	Confirmed
WASP14 /BD+22 2716	1	1.451 +/- 0.007	232.16 +/- 29.00	Confirmed
WASP20	1	0.2569 +/- 0.0002	53.9 +/- 5.0	Not confirmed
WASP-179	1	0.648 +/- 0.014	233.4 +/- 7.0	Not confirmed
HATS776-001/HATS24	1	0.400 +/- 0.009	204 +/- 7	Not confirmed
HATS700-028/	1	0.39 +/- 0.11	215 +/- 60	Not confirmed
HAT-P-41	1	3.64 +/- 0.17	1279.9 +/- 62.0	Confirmed

*Nc is the number of candidate companions.

CHAPTER IV

CONCLUSION

We performed a high-resolution direct imaging survey using Adaptive Optics on eighteen stars where eleven of them are known hosts to transiting hot Jupiters with spin-orbit misalignment. Our sample has host star magnitudes of 5-12 at V filter and distance range of 10-500 pc as they were all included in ground-based transit searches like HATnet and WASP. We detected eleven companions around these targets and we could report five new stellar companion candidates. We could validate or/and confirm five candidates in our sample. We could also prove one companion is a background object. Table 3.1 shows all these targets with the separation of their candidates.

Figure 4.1 presents a polar scatter chart of spin-orbit obliquity versus separation that is a combination of our targets and the targets presented by Ngo et al. (2015;2016) to investigate a bigger sample of the hot Jupiter systems with candidates. Although we increased the sample by using Ngo et al. (2015;2016) targets in the chart, we still believe our sample size is not large enough to prove any correlation between the misalignment in spin orbit of the hot Jupiters and presence of a distance stellar companion.

Due to COVID-19, our attempts to obtain more observations for our data were unsuccessful (Palomar observatory canceled all the proposals for a semester). The next step for us is to obtain follow up observations on the five new reported candidate companions and confirm whether they are gravitationally bound to the system. We have several stars with known measurements of spin-orbit obliquity that we will add to our sample to be able to find any correlation between the spin-

orbit obliquity and the hot Jupiter's properties. Also, with increasing the sample size to one hundred stars, we are hoping to find a relationship between the separation of the stellar companion and the value of spin-orbit obliquity and investigate if closer companion can cause more spin-orbit obliquity in the hot Jupiters. With a sample of more than one hundred stars, we would have the opportunity to investigate the Kozai-Lidov effect in the misaligned hot Jupiters properly. Also, we can explore how the Kozai mechanism influenced the final semi-major axis of hot Jupiters after the migration and estimate a more precise range of semi-major axes of the hot Jupoters in which have the most impact.
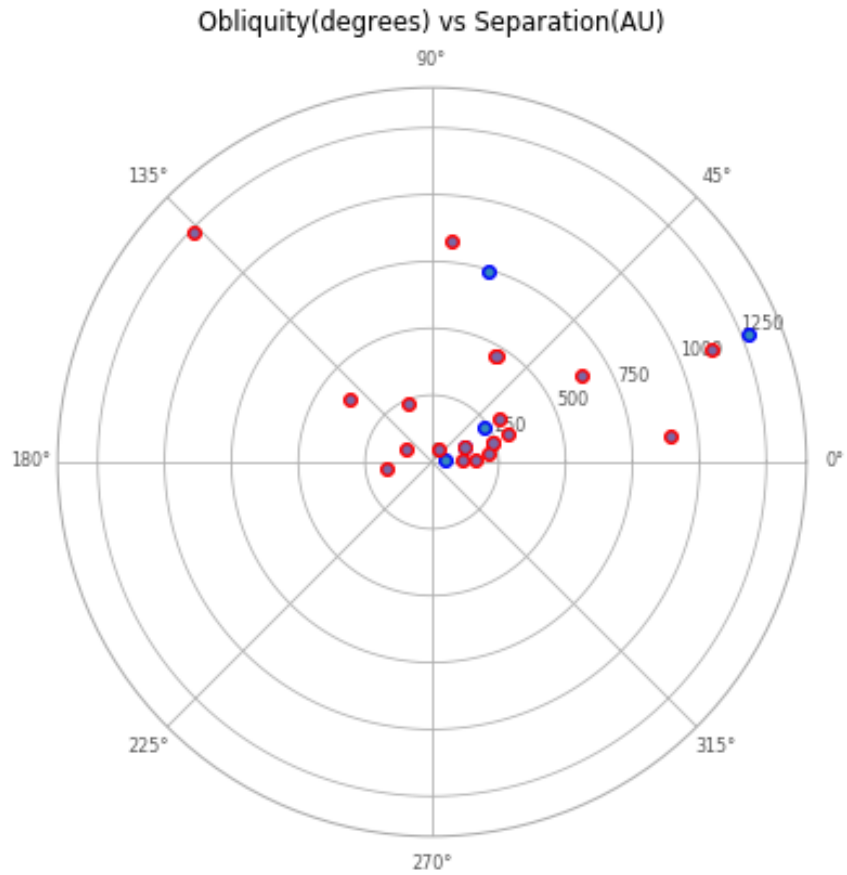
Figure 4.1   Spin-Orbit Obliquity versus Separation polar chart. The blue data points in the chart are results of this work. The red data points are from Ngo et al. (2015;2016)

REFERENCES

Adams, E. R., Dupree, A. K., Kulesa, C., & McCarthy, D. (2013). ADAPTIVE OPTICS IMAGES. II. 12 *KEPLER* OBJECTS OF INTEREST AND 15 CONFIRMED TRANSITING PLANETS. *The Astronomical Journal*, *146*(1), 9. https://doi.org/10.1088/0004-6256/146/1/9

Adams, F. C., & Laughlin, G. (2006). Effects of Secular Interactions in Extrasolar Planetary Systems. *The Astrophysical Journal*, *649*(2), 992–1003. https://doi.org/10.1086/506142

Addison, B. C., Wang, S., Johnson, M. C., Tinney, C. G., Wright, D. J., & Bayliss, D. (2018). Stellar Obliquities & Planetary Alignments (SOPA) I. Spin-Orbit measurements of Three Transiting Hot Jupiters: WASP-72b, WASP-100b, & WASP-109b. *The Astronomical Journal*, *156*(5), 197. https://doi.org/10.3847/1538-3881/aade91

Albrecht, S., Winn, J. N., Butler, R. P., Crane, J. D., Shectman, S. A., Thompson, I. B., Hirano, T., & Wittenmyer, R. A. (2012). A High Stellar Obliquity in the WASP-7 Exoplanetary System. *The Astrophysical Journal*, *744*, 189. https://doi.org/10.1088/0004-637X/744/2/189

Anderson, D. R., Bouchy, F., Brown, D. J. A., Burdanov, A., Cameron, A. C., Delrez, L., Gillon, M., Hellier, C., Jehin, E., Lendl, M., Maxted, P. F. L., Nielsen, L. D., Pepe, F., Pollacco, D., Queloz, D., Ségransan, D., Smalley, B., Temple, L. Y., Triaud, A. H. M. J., … West, R. G. (2018). A low-density hot Jupiter in a near-aligned, 4.5-day orbit around a V = 10.8, F5V star. *ArXiv:1809.07709 [Astro-Ph]*. http://arxiv.org/abs/1809.07709

Anderson, D. R., Brown, D. J. A., Cameron, A. C., Delrez, L., Fumel, A., Gillon, M., Hellier, C., Jehin, E., Lendl, M., Maxted, P. F. L., Neveu-VanMalle, M., Pepe, F., Pollacco, D., Queloz, D., Rojo, P., Segransan, D., Serenelli, A. M., Smalley, B., Smith, A. M. S., … West, R. G. (2014). Six newly-discovered hot Jupiters transiting F/G stars: WASP-87b, WASP-108b, WASP-109b, WASP-110b, WASP-111b & WASP-112b. *ArXiv:1410.3449 [Astro-Ph]*. http://arxiv.org/abs/1410.3449

Anderson, D. R., Collier Cameron, A., Hellier, C., Lendl, M., Lister, T. A., Maxted, P. F. L., Queloz, D., Smalley, B., Smith, A. M. S., Triaud, A. H. M. J., Brown, D. J. A., Gillon, M., Neveu-VanMalle, M., Pepe, F., Pollacco, D., Ségransan, D., Udry, S., West, R. G., & Wheatley, P. J. (2015). WASP-20b and WASP-28b: A hot Saturn and a hot Jupiter in near-aligned orbits around solar-type stars. *Astronomy and Astrophysics*, *575*, A61. https://doi.org/10.1051/0004-6361/201423591

Beaugé, C., & Nesvorný, D. (2012). EMERGING TRENDS IN A PERIOD-RADIUS DISTRIBUTION OF CLOSE-IN PLANETS. *The Astrophysical Journal*, *763*(1), 12. https://doi.org/10.1088/0004-637X/763/1/12

Béky, B., Bakos, G. Á., Hartman, J., Torres, G., Latham, D. W., Jordán, A., Arriagada, P., Bayliss, D., Kiss, L. L., Kovács, G., Quinn, S. N., Marcy, G. W., Howard, A. W., Fischer, D. A., Johnson, J. A., Esquerdo, G. A., Noyes, R. W., Buchhave, L. A., Sasselov, D. D., … Sári, P. (2011). HAT-P-27b: A hot Jupiter transiting a G star on a 3 day orbit. *The Astrophysical Journal*, *734*(2), 109. https://doi.org/10.1088/0004-637X/734/2/109

Bento, J., Schmidt, B., Hartman, J. D., Bakos, G. Á., Ciceri, S., Brahm, R., Bayliss, D., Espinoza, N., Zhou, G., Rabus, M., Bhatti, W., Penev, K., Csubry, Z., Jordán, A., Mancini, L., Henning, T., de Val-Borro, M., Tinney, C. G., Wright, D. J., … Sári, P. (2017). HATS-22b, HATS-23b and HATS-24b: Three new transiting super-Jupiters from the HATSouth project. *Monthly Notices of the Royal Astronomical Society*, *468*, 835–848. https://doi.org/10.1093/mnras/stx500

Blecic, J., Harrington, J., Madhusudhan, N., Stevenson, K. B., Hardy, R. A., Cubillos, P., Hardin, M., Campo, C. J., Bowman, W. C., Nymeyer, S., Loredo, T. J., Anderson, D. R., & Maxted, P. F. L. (2013). Thermal Emission of WASP-14b Revealed with Three Spitzer Eclipses. *The Astrophysical Journal*, *779*(1), 5. https://doi.org/10.1088/0004-637X/779/1/5

Bohn, A. J., Southworth, J., Ginski, C., Kenworthy, M. A., Maxted, P. F. L., & Evans, D. F. (2020). A multiplicity study of transiting exoplanet host stars—I. High-contrast imaging with VLT/SPHERE. *Astronomy & Astrophysics*, *635*, A73. https://doi.org/10.1051/0004-6361/201937127

Bonomo, A. S., Desidera, S., Benatti, S., Borsa, F., Crespi, S., Damasso, M., Lanza, A. F., Sozzetti, A., Lodato, G., Marzari, F., Boccato, C., Claudi, R. U., Cosentino, R., Covino, E., Gratton, R., Maggio, A., Micela, G., Molinari, E., Pagano, I., … Scandariato, G. (2017). The GAPS Programme with HARPS-N at TNG. XIV. Investigating giant planet migration history via improved eccentricity and mass determination for 231 transiting planets. *Astronomy and Astrophysics*, *602*, A107. https://doi.org/10.1051/0004-6361/201629882

Brown, D. J. A., Collier Cameron, A., Díaz, R. F., Doyle, A. P., Gillon, M., Lendl, M., Smalley, B., Triaud, A. H. M. J., Anderson, D. R., Enoch, B., Hellier, C., Maxted, P. F. L., Miller, G. R. M., Pollacco, D., Queloz, D., Boisse, I., & Hébrard, G. (2012). Analysis of Spin-Orbit Alignment in the WASP-32, WASP-38, and HAT-P-27/WASP-40 Systems. *The Astrophysical Journal*, *760*, 139. https://doi.org/10.1088/0004-637X/760/2/139

Carrera, D., Raymond, S. R., & Davies, M. B. (2019). Planet-planet scattering as the source of the highest eccentricity exoplanets. *ArXiv Preprint ArXiv:1903.02564*.

Chaplin, W. J., Basu, S., Huber, D., Serenelli, A., Casagrande, L., Aguirre, V. S., Ball, W. H., Creevey, O. L., Gizon, L., & Handberg, R. (2013). Asteroseismic fundamental properties of solar-type stars observed by the NASA Kepler mission. *The Astrophysical Journal Supplement Series*, *210*(1), 1.

Chatterjee, S., Ford, E. B., Matsumura, S., & Rasio, F. A. (2008). Dynamical outcomes of planet-planet scattering. *The Astrophysical Journal*, *686*(1), 580.

Chauvin, G., Lagrange, A.-M., Zuckerman, B., Dumas, C., Mouillet, D., Song, I., Beuzit, J.-L., Lowrance, P., & Bessell, M. S. (2005). A companion to AB Pic at the planet/brown dwarf boundary. *Astronomy & Astrophysics*, *438*(3), L29–L32.

Dawson, R. I., & Johnson, J. A. (2018). Origins of Hot Jupiters. *Annual Review of Astronomy and Astrophysics*, *56*, 175–221.

Dawson, R. I., & Murray-Clay, R. A. (2013). Giant planets orbiting metal-rich stars show signatures of planet-planet interactions. *The Astrophysical Journal Letters*, *767*(2), L24.

Désert, J.-M., Bean, J., Kempton, E. M.-R., Berta, Z. K., Charbonneau, D., Irwin, J., Fortney, J., Burke, C. J., & Nutzman, P. (2011). Observational evidence for a metal-rich atmosphere on the super-Earth GJ1214b. *The Astrophysical Journal Letters*, *731*(2), L40.

Dong, S., Katz, B., & Socrates, A. (2013). WARM JUPITERS NEED CLOSE "FRIENDS" FOR HIGH-ECCENTRICITY MIGRATION—A STRINGENT UPPER LIMIT ON THE PERTURBER'S SEPARATION. *The Astrophysical Journal Letters*, *781*(1), L5.

Enoch, B., Anderson, D. R., Barros, S. C. C., Brown, D. J. A., Cameron, A. C., Faedi, F., Gillon, M., Hébrard, G., Lister, T. A., Queloz, D., Santerne, A., Smalley, B., Street, R. A., Triaud, A. H. M. J., West, R. G., Bouchy, F., Bento, J., Butters, O., Fossati, L., … Wheatley, P. J. (2011). WASP-35b, WASP-48b and WASP-51b: Two new planets and an independent discovery of HAT-P-30b. *The Astronomical Journal*, *142*(3), 86. https://doi.org/10.1088/0004-6256/142/3/86

Evans, D. F., Southworth, J., Maxted, P. F. L., Skottfelt, J., Hundertmark, M., Jørgensen, U. G., Dominik, M., Alsubai, K. A., Andersen, M. I., & Bozza, V. (2016). High-resolution Imaging of Transiting Extrasolar Planetary systems (HITEP)-I. Lucky imaging observations of 101 systems in the southern hemisphere. *Astronomy & Astrophysics*, *589*, A58.

Evans, D., Southworth, J., & Smalley, B. (2016). WASP-20 is a close visual binary with a transiting hot Jupiter. *ArXiv Preprint ArXiv:1611.08735*.

Fogg, M. J., & Nelson, R. P. (2007). Can Terrestrial Planets Form in Hot-Jupiter Systems? *ArXiv Preprint ArXiv:0710.3730*.

Fontanive, C., Rice, K., Bonavita, M., Lopez, E., Mužić, K., & Biller, B. (2019). A high binary fraction for the most massive close-in giant planets and brown dwarf desert members. *Monthly Notices of the Royal Astronomical Society*, *485*(4), 4967–4996. https://doi.org/10.1093/mnras/stz671

Gonzalez, C. A. G., Wertz, O., Absil, O., Christiaens, V., Defrère, D., Mawet, D., Milli, J., Absil, P.-A., Van Droogenbroeck, M., & Cantalloube, F. (2017). Vip: Vortex image processing package for high-contrast direct imaging. *The Astronomical Journal*, *154*(1), 7.

Johnson, J. A., Winn, J. N., Albrecht, S., Howard, A. W., Marcy, G. W., & Gazak, J. Z. (2009). A Third Exoplanetary System with Misaligned Orbital and Stellar Spin Axes. *Publications of the Astronomical Society of the Pacific*, *121*, 1104. https://doi.org/10.1086/644604

Johnson, J. A., Winn, J. N., Hartman, J. D., Bakos, G. A., Morton, T. D., Torres, G., Kovács, G., Latham, D. W., Noyes, R. W., Sato, B., Esquerdo, G. A., Fischer, D. A., Marcy, G. W., Howard, A. W., Quinn, S. N., Beky, B., Sasselov, D. D., Stefanik, R. P., Lazar, J., … Furesz, G. (2011). HAT-P-30b: A transiting hot Jupiter on a highly oblique orbit. *The Astrophysical Journal*, *735*(1), 24. https://doi.org/10.1088/0004-637X/735/1/24

Johnson, M. C., Cochran, W. D., Addison, B. C., Tinney, C. G., & Wright, D. J. (2017a). Spin–Orbit Misalignments of Three Jovian Planets via Doppler Tomography. *The Astronomical Journal*, *154*(4), 137.

Johnson, M. C., Cochran, W. D., Addison, B. C., Tinney, C. G., & Wright, D. J. (2017b). Spin-Orbit Misalignments of Three Jovian Planets via Doppler Tomography. *The Astronomical Journal*, *154*, 137. https://doi.org/10.3847/1538-3881/aa8462

Joshi, Y. C., Pollacco, D., Collier Cameron, A., Skillen, I., Simpson, E., Steele, I., Street, R. A., Stempels, H. C., Christian, D. J., Hebb, L., Bouchy, F., Gibson, N. P., Hébrard, G., Keenan, F. P., Loeillet, B., Meaburn, J., Moutou, C., Smalley, B., Todd, I., … Wilson, D. M. (2009). WASP-14b: 7.3 MJ transiting planet in an eccentric orbit. *Monthly Notices of the Royal Astronomical Society*, *392*, 1532–1538. https://doi.org/10.1111/j.1365-2966.2008.14178.x

Ketchum, J. A., Adams, F. C., & Bloch, A. M. (2011). Accretion of Rocky Planets by Hot Jupiters. *The Astrophysical Journal Letters*, *741*(1), L2.

Knutson, H. A., Fulton, B. J., Montet, B. T., Kao, M., Ngo, H., Howard, A. W., Crepp, J. R., Hinkley, S., Bakos, G. Á., & Batygin, K. (2014). Friends of hot Jupiters. I. A radial velocity search for massive, long-period companions to close-in gas giant planets. *The Astrophysical Journal*, *785*(2), 126.

Kozai, Y. (1962). Secular perturbations of asteroids with high inclination and eccentricity. *The Astronomical Journal*, *67*, 591.

Lidov, M. L. (1962). The evolution of orbits of artificial satellites of planets under the action of gravitational perturbations of external bodies. *Planetary and Space Science*, *9*(10), 719–759.

Males, J. R., Close, L. M., Morzinski, K. M., Wahhaj, Z., Liu, M. C., Skemer, A. J., Kopon, D., Follette, K. B., Puglisi, A., & Esposito, S. (2014). Magellan adaptive optics first-light observations of the exoplanet β pic b. I. direct imaging in the far-red optical with MagAO+ VisAO and in the near-ir with nici. *The Astrophysical Journal*, *786*(1), 32.

Mayor, M., & Queloz, D. (1995). A Jupiter-mass companion to a solar-type star. *Nature*, *378*(6555), 355–359.

Mazeh, T., Holczer, T., & Shporer, A. (2015). Time Variation of Kepler Transits Induced By Stellar Rotating Spots—A Way to Distinguish between Prograde and Retrograde Motion. I. Theory. *The Astrophysical Journal*, *800*(2), 142.

Mazeh, T., Perets, H. B., McQuillan, A., & Goldstein, E. S. (2015). Photometric Amplitude Distribution of Stellar Rotation of KOIs—Indication for Spin-Orbit Alignment of Cool Stars and High Obliquity for Hot Stars. *The Astrophysical Journal*, *801*(1), 3.

Mordasini, C., Mollière, P., Dittkrist, K.-M., Jin, S., & Alibert, Y. (2015). Global models of planet formation and evolution. *International Journal of Astrobiology*, *14*(2), 201–232.

Morzinski, K. M. (2014). *Linearity Correction for Clio Instrument*.

Morzinski, K. M., Males, J. R., Skemer, A. J., Close, L. M., Hinz, P. M., Rodigas, T. J., Puglisi, A., Esposito, S., Riccardi, A., & Pinna, E. (2015). Magellan adaptive optics first-light observations of the exoplanet β Pic b. II. 3–5 μm direct imaging with MagAO+ Clio, and the empirical bolometric luminosity of a self-luminous giant planet. *The Astrophysical Journal*, *815*(2), 108.

Mustill, A. J., Davies, M. B., & Johansen, A. (2015). The Destruction of Inner Planetary Systems during High-eccentricity Migration of Gas Giants. *The Astrophysical Journal*, *808*, 14. https://doi.org/10.1088/0004-637X/808/1/14

Naoz, S. (2016). The eccentric Kozai-Lidov effect and its applications. *Annual Review of Astronomy and Astrophysics*, *54*, 441–489.

Naoz, S., Farr, W. M., Lithwick, Y., Rasio, F. A., & Teyssandier, J. (2011). Hot Jupiters from secular planet–planet interactions. *Nature*, *473*(7346), 187–189.

Naoz, S., Farr, W. M., & Rasio, F. A. (2012). On the formation of hot Jupiters in stellar binaries. *The Astrophysical Journal Letters*, *754*(2), L36.

Ngo, H., Knutson, H. A., Hinkley, S., Bryan, M., Crepp, J. R., Batygin, K., Crossfield, I., Hansen, B., Howard, A. W., & Johnson, J. A. (2016). FRIENDS OF HOT JUPITERS. IV. STELLAR COMPANIONS BEYOND 50 au MIGHT FACILITATE GIANT PLANET FORMATION, BUT MOST ARE UNLIKELY TO CAUSE KOZAI–LIDOV MIGRATION. *The Astrophysical Journal*, *827*(1), 8.

Ngo, H., Knutson, H. A., Hinkley, S., Crepp, J. R., Bechter, E. B., Batygin, K., Howard, A. W., Johnson, J. A., Morton, T. D., & Muirhead, P. S. (2015). Friends of hot Jupiters. II. No correspondence between hot-Jupiter spin-orbit misalignment and the incidence of directly imaged stellar companions. *The Astrophysical Journal*, *800*(2), 138.

Ogihara, M., Kobayashi, H., & Inutsuka, S. (2014). N-body simulations of terrestrial planet formation under the influence of a hot jupiter. *The Astrophysical Journal*, *787*(2), 172.

Pepe, F., Correia, A. C. M., Mayor, M., Tamuz, O., Couetdic, J., Benz, W., Bertaux, J.-L., Bouchy, F., Laskar, J., Lovis, C., Naef, D., Queloz, D., Santos, N. C., Sivan, J.-P., Sosnowska, D., & Udry, S. (2007). The HARPS search for southern extra-solar planets: VIII. μ Arae, a system with four planets. *Astronomy & Astrophysics*, *462*(2), 769–776. https://doi.org/10.1051/0004-6361:20066194

Podolak, M., & Zucker, S. (2004). A note on the snow line in protostellar accretion disks. *Meteoritics & Planetary Science*, *39*(11), 1859–1868.

Pont, F., Hébrard, G., Irwin, J. o, Bouchy, F., Moutou, C., Ehrenreich, D., Guillot, T., Aigrain, S., Bonfils, X., & Berta, Z. (2009). Spin-orbit misalignment in the HD 80606 planetary system. *Astronomy & Astrophysics*, *502*(2), 695–703.

Queloz, D., Eggenberger, A., Mayor, M., Perrier, C., Beuzit, J. L., Naef, D., Sivan, J. P., & Udry, S. (2000). Detection of a spectroscopic transit by the planet orbiting the star HD209458. *ArXiv Preprint Astro-Ph/0006213*.

Sanchis-Ojeda, R., & Winn, J. N. (2011). Starspots, spin-orbit misalignment, and active latitudes in the HAT-P-11 exoplanetary system. *The Astrophysical Journal*, *743*(1), 61.

Southworth, J., Dominik, M., Jorgensen, U. G., Rahvar, S., Snodgrass, C., Alsubai, K., Bozza, V., Browne, P., Burgdorf, M., Novati, S. C., Dodds, P., Dreizler, S., Finet, F., Gerner, T., Hardis, S., Harpsoe, K., Hellier, C., Hinse, T. C., Hundertmark, M., … Surdej, J. (2011). A much lower density for the transiting extrasolar planet WASP-7. *Astronomy & Astrophysics*, *527*, A8. https://doi.org/10.1051/0004-6361/201016183

Stassun, K. G., Collins, K. A., & Gaudi, B. S. (2017). Accurate Empirical Radii and Masses of Planets and Their Host Stars with Gaia Parallaxes. *The Astronomical Journal*, *153*, 136. https://doi.org/10.3847/1538-3881/aa5df3

Stello, D., Huber, D., Bedding, T. R., Benomar, O., Bildsten, L., Elsworth, Y. P., Gilliland, R. L., Mosser, B., Paxton, B., & White, T. R. (2013). Asteroseismic classification of stellar populations among 13,000 red giants observed by Kepler. *The Astrophysical Journal Letters*, *765*(2), L41.

Storch, N. I., Anderson, K. R., & Lai, D. (2014). Chaotic dynamics of stellar spin in binaries and the production of misaligned hot Jupiters. *Science*, *345*(6202), 1317–1321.

Triaud, A. H. M. J., Collier Cameron, A., Queloz, D., Anderson, D. R., Gillon, M., Hebb, L., Hellier, C., Loeillet, B., Maxted, P. F. L., Mayor, M., Pepe, F., Pollacco, D., Ségransan, D., Smalley, B., Udry, S., West, R. G., & Wheatley, P. J. (2010). Spin-orbit angle measurements for six southern transiting planets. New insights into the dynamical origins of hot Jupiters. *Astronomy and Astrophysics*, *524*, A25. https://doi.org/10.1051/0004-6361/201014525

Triaud, Amaury H. M. J., Anderson, D. R., Cameron, A. C., Doyle, A. P., Fumel, A., Gillon, M., Hellier, C., Jehin, E., Lendl, M., Lovis, C., Maxted, P. F. L., Pepe, F., Pollacco, D., Queloz, D., Segransan, D., Smalley, B., Smith, A. M. S., Udry, S., West, R. G., & Wheatley, P. J. (2013). WASP-80b: A gas giant transiting a cool dwarf. *Astronomy & Astrophysics*, *551*, A80. https://doi.org/10.1051/0004-6361/201220900

Triaud, Amaury H. M. J., Gillon, M., Ehrenreich, D., Herrero, E., Lendl, M., Anderson, D. R., Collier Cameron, A., Delrez, L., Demory, B.-O., Hellier, C., Heng, K., Jehin, E., Maxted, P. F. L., Pollacco, D., Queloz, D., Ribas, I., Smalley, B., Smith, A. M. S., & Udry, S. (2015a). WASP-80b has a dayside within the T-dwarf range. *Monthly Notices of the Royal Astronomical Society*, *450*, 2279–2290. https://doi.org/10.1093/mnras/stv706

Triaud, Amaury H. M. J., Gillon, M., Ehrenreich, D., Herrero, E., Lendl, M., Anderson, D. R., Collier Cameron, A., Delrez, L., Demory, B.-O., Hellier, C., Heng, K., Jehin, E., Maxted, P. F. L., Pollacco, D., Queloz, D., Ribas, I., Smalley, B., Smith, A. M. S., & Udry, S. (2015b). WASP-80b has a dayside within the T-dwarf range. *Monthly Notices of the Royal Astronomical Society*, *450*, 2279–2290. https://doi.org/10.1093/mnras/stv706

Van Eylen, V., Lund, M. N., Aguirre, V. S., Arentoft, T., Kjeldsen, H., Albrecht, S., Chaplin, W. J., Isaacson, H., Pedersen, M. G., & Jessen-Hansen, J. (2014). What asteroseismology can do for exoplanets: Kepler-410A b is a small Neptune around a bright star, in an eccentric orbit consistent with low obliquity. *The Astrophysical Journal*, *782*(1), 14.

Winn, J. N., Fabrycky, D., Albrecht, S., & Johnson, J. A. (2010). Hot stars with hot Jupiters have high obliquities. *The Astrophysical Journal Letters*, *718*(2), L145.

Winn, J. N., & Fabrycky, D. C. (2015). The occurrence and architecture of exoplanetary systems. *Annual Review of Astronomy and Astrophysics*, *53*, 409–447.

Wöllert, M., & Brandner, W. (2015). A Lucky Imaging search for stellar sources near 74 transit hosts. *Astronomy & Astrophysics*, *579*, A129.

Wu, Y., & Lithwick, Y. (2011). Secular chaos and the production of hot Jupiters. *The Astrophysical Journal*, *735*(2), 109.

Wu, Y., Murray, N. W., & Ramsahai, J. M. (2007). Hot Jupiters in binary star systems. *The Astrophysical Journal*, *670*(1), 820.